Passive Tension and Stiffness of Vertebrate Skeletal and Insect Flight Muscles: The Contribution of Weak Cross-bridges and Elastic Filaments

Henk L. M. Granzier* and Kuan Wang
Department of Chemistry and Biochemistry, Biochemical Institute, University of Texas at Austin, Austin, Texas 78712 USA

ABSTRACT Tension and dynamic stiffness of passive rabbit psoas, rabbit semitendinosus, and waterbug indirect flight muscles were investigated to study the contribution of weak-binding cross-bridges and elastic filaments (titin and minititin) to the passive mechanical behavior of these muscles. Experimentally, a functional dissection of the relative contribution of actomyosin cross-bridges and titin and minititin was achieved by 1) comparing mechanically skinned muscle fibers before and after selective removal of actin filaments with a noncalcium-requiring gelsolin fragment (FX-45), and 2) studying passive tension and stiffness as a function of sarcomere length, ionic strength, temperature, and the inhibitory effect of a carboxyl-terminal fragment of smooth muscle caldesmon.

Our data show that weak bridges exist in both rabbit skeletal muscle and insect flight muscle at physiological ionic strength and room temperature. In rabbit psoas fibers, weak bridge stiffness appears to vary with both thin-thick filament overlap and with the magnitude of passive tension. Plots of passive tension versus passive stiffness are multiphasic and strikingly similar for these three muscles of distinct sarcomere proportions and elastic proteins. The tension-stiffness plot appears to be a powerful tool in discerning changes in the mechanical behavior of the elastic filaments. The stress-strain and stiffness-strain curves of all three muscles can be merged into one, by normalizing strain rate and strain amplitude of the extensible segment of titin and minititin, further supporting the segmental extension model of resting tension development.

INTRODUCTION

The giant proteins titin and nebulin are major components of an endosarcomeric matrix that provides structural support and mechanical integration of the interdigitating myosin and actin filaments in the contractile machinery of skeletal muscle (for reviews see Wang (1985), Maruyama (1986), and Trinick (1991)). Titin is a giant elastic protein with size variants ranging from 2.1 to 3.5 MDa. Each titin polypeptide (1 μm in length) spans a half sarcomere from the Z-line to the M-line and consists of two mechanical segments: a segment between the Z-line and the edge of the A band that is extensible and serves as an elastic molecular spring, and a segment within the A band that is anchored and inextensible, presumably by its interaction with thick filaments.

A family of related proteins, twitchin, projectin, and minititin, with reported sizes from 0.6 to 1.2 MDa, is found in invertebrate flight and skeletal muscles (Benian et al., 1989; Nave and Weber, 1990; Lakey et al., 1990; Hu et al., 1990; Nave et al., 1991; Ayme-Southgate et al., 1991). Minititin of insect indirect flight muscle (IFM) is about 260 nm long and spans from the Z-line to the outer region of the A band (Nave and Weber, 1990) and is thought to make up the elastic C filament that connects the end of the thick filaments to the Z-lines in insect IFM fibers (Reedy, 1971; White and Thorson, 1973; Trombitás and Tigyi-Sébes, 1979).

Recent mechanical studies of single muscle fibers indicate that the degree of extension of the extensible segment of titin in vertebrate muscle (Wang et al., 1991, 1993) and the C filament in insect IFM (Granzier et al., 1993A) is an important parameter in understanding the stress-strain curves of resting (or nonactivated) muscles. The anchored A band segment of titin may serve as a template protein that determines the length of the myosin thick filament (Wang, 1985), a proposal supported by sequence analysis of titin (Labeit et al., 1992).

Nebulin, a distinct family of giant proteins, with size variants from 0.7 to 0.9 MDa, is an integral component of the thin filaments of skeletal muscle (Wang and Williamson, 1980; Wang and Wright, 1988; Kruger et al., 1991). It attaches at its carboxyl terminus to the Z-line and appears to behave as a length determining protein ruler for the actin filament, by binding along its length (Jin and Wang, 1991; Wright et al., manuscript 1993.).

To explore the functional roles of each of the four filamentous systems in the sarcomere, selective removal of one or more of the filament types is an effective approach. Manipulation of ionic strength has been successfully applied to remove or partially truncate myosin filaments (Higuchi et al., 1992). A powerful technique for selective removal of actin filaments from sarcomeres of skeletal muscle by the protein gelsolin was introduced by Funatsu et al. (1990). We have recently applied this technique to reveal the interplay between passive tension and strong and weak cross-bridges in insect IFM (Granzier and Wang, 1993a). During the course of this work we observed that the calcium that is required for

Received for publication 18 May 1993 and in final form 19 July 1993.

Address reprint requests to Dr. Kuan Wang, Welch 4.230 C, Department of Chemistry and Biochemistry, University of Texas at Austin, Austin, TX 78712.

* Present address: Department of Veterinary Comparative Anatomy, Pharmacology and Physiology, College of Veterinary Medicine, Washington State University, Pullman, WA 99164-6520.

0006-3495/93/11/2141/19 $2.00

optimal actin-severing activity of intact gelsolin would occasionally induce proteolysis and cause structural damage that complicates interpretation (see also Funatsu et al. (1990) and Kruger et al. (1991)) To alleviate this problem we have substituted intact gelsolin with an amino-terminal gelsolin fragment, FX-45 (45 kDa), which severs actin filaments effectively in the absence of calcium (Yu et al., 1991). Furthermore, its smaller size facilitates accessibility to actin filaments.

We report in this paper the application of the FX-45-mediated actin filament removal technique and the evaluation of the relative contribution of weak cross-bridges to the passive stiffness of resting muscles by measuring ionic strength dependence of stiffness before and after actin filament removal, and by measuring the sensitivity of stiffness to a carboxyl-terminal fragment of smooth muscle caldesmon which inhibits actomyosin interaction. We investigated further the segmental extension model of passive tension (Wang et al., 1991, 1993) by measuring, with carefully controlled stretch-release protocols, passive tension-sarcomere length curves of psoas and semitendinosus muscles from the rabbit and IFM from the waterbug *Lethocerus*.

MATERIALS AND METHODS

Muscle fibers

Insect IFM fibers were prepared from both fresh (<2 h postmortem) and glycerinated dorso longitudinal muscle of *Lethocerus griseus* and *Lethocerus uhleri*, as described in Granzier and Wang (1993a). For rabbit muscles, small bundles of about 500 fibers were quickly removed from psoas and semitendinosus tissues of exsanguinated New Zealand rabbits, stretched between 0 and 10%, and tied to glass rods. The rods were immersed in 40 ml of relaxing solution (50 mM potassium propionate; 50 mM imidazole, 7.0 mM Mg acetate, 6.0 mM ATP, 20 mM EGTA, 1 mM dithiothreitol (DTT), 2 mM diisopropylfluorophosphate (DIFP), 0.5 mM phenylmethenesulfonyl fluoride (PMSF), 20 μg/ml leupeptin, 0.5% (w/v) of purified Triton X-100 (28314; Pierce Chemical Co., Rockford, IL) pH 7.0 at 4°C) for 30 min, and then transferred to Triton-free relaxing solution. The bundles were used immediately to prepare single fibers as described in Granzier and Wang (1993b). To avoid calcium contamination, dissection tools and containers were washed with 0.5 M EGTA (pH 7.6) and rinsed with relaxing solution.

Myofibrils

Myofibrils were prepared at 4°C, less than 2 h postmortem. To prepare IFM myofibrils, fiber bundles in relaxing solution were minced using a scalpel and passed twice, each time, through syringe needles of decreasing bore size (16, 21, and 23 gauge; 1-inch long). The mince was spun in a clinical centrifuge at top speed for 10 min (model CL; IEC, Needham HTS, MA). Myofibrils in the loose pellet were gently resuspended in relaxing solution, spun, and resuspended again. The suspension contained long straight myofibrils that had distinct A and *I* bands in phase contrast microscopy. Myofibril suspension were settled onto glass coverslips (acid-washed and alcohol-cleaned) in a moisture box for 1 h and were used for extraction experiments (see below).

Rabbit psoas myofibrils were prepared from fiber bundles that had been stretched 50% in relaxing solution, tied to glass rods, and put in rigor solution (70 mM potassium propionate; 50 mM imidazole, 1.0 mM magnesium acetate, 20 mM EGTA, 1 mM DTT, 2 mM DIFP, 0.5 mM PMSF, 20 μg/ml leupeptin 0.5% triton, pH 7.0 at 0°C) that was refreshed five times (to wash out ATP). A fiber bundle (~500 fibers, 2–3 cm long, in 10 ml of rigor solution) was cut into small pieces and blended in a Virtis Model 23 blade homogenizer (Virtis Co., Inc., Gardiner, NY) for 20 s at top speed. The mince was spun in the clinical centrifuge, the pellet was gently resuspended in rigor solution, and myofibril suspension was added to glass coverslips and placed in a moisture box for 1 h. Rigor solution was replaced by relaxing solution and myofibrils were used for experiments with FX-45.

Gelsolin fragment (FX-45) and thin-filament removal

The gelsolin clone, FX-45, was a kind gift from Dr. Helen Yin (University of Texas Southwestern Medical Center, Dallas), and contained the amino-terminal half (amino acids 1–406) of human gelsolin cDNA constructed in a PET3d expression vector. Expression and purification was according to Yu et al. (1991) with some modifications (Huang, Guttierez, and Wang, unpublished observations). FX-45 was dialyzed into buffer A (10 mM 4-morpholinepropanesulfonic acid; 10 mM EGTA; 1.0 mM magnesium acetate; 20 mM potassium propionate; 1 mM DTT; 20 μg/ml leupeptin; pH 7.0 at 21–23°C). Protein concentrations were measured using the Bio-Rad protein assay (500-0006; Bio-Rad Laboratories, Richmond, CA), with bovine serum albumin as the standard. The sample was then aliquoted and quick-frozen in liquid nitrogen and stored at −70°C. On the day of use, an aliquot was thawed (37°C) and spun for 5 min in a microcentrifuge (Fisher model 59, 12,600 rpm). The protein was mixed with a half volume of a relaxing buffer containing: 10 mM 4-morpholinepropanesulfonic acid; 1.0 mM EGTA; 15 mM magnesium acetate; 12 mM ATP; 245 mM potassium propionate; and 150 μg/ml leupeptin; pH 7.0 at 21–23°C.

To extract thin filaments with FX-45, fiber segments (3 mm long) in relaxing solution were pinned down with fine needles in 50-μl troughs made in the Sylgard base of a small dissection dish. FX-45 was then added at 10 molar excess (5 μg of FX-45/mm of fiber). The dissection dish was placed inside a closed large petri dish containing wet filter paper and affixed to the top of a vortexer set at 60 rpm. After incubating at room temperature for certain durations, the solution was removed from each trough, while the fiber was extensively washed for 10–20 min by replacing the solution in the trough five times with relaxing solution. Fibers and extracts were analyzed by sodium dodecyl sulfate (SDS) gel electrophoresis (see below). Some fibers were cut in half, one half was used for SDS-polyacrylamide gel electrophoresis analysis and the other half for actin localization studies with confocal microscopy.

Thin-filament extraction from myofibrils was done by adding FX-45 to the side of coverslips to which the myofibrils adhered. Coverslips were incubated in a moisture box at 21–23°C. After various times of extraction, coverslips were washed with relaxing solution.

Caldesmon fragment

The carboxyl-terminal fragment (27 kDa) of chicken gizzard caldesmon expressed in *Escherichia coli* as a CII-caldesmon fusion protein with caldesmon sequence beginning at Lys^{579} (Wang et al., 1991) was a kind gift of Dr. Albert Wang (Boston Medical Research Institute, Boston). The fragment was dialyzed into solution B (15 mM potassium propionate, 1.0 mM EGTA, 10 mM imidazole, 20 μg/ml leupeptin, and pH 7.0 at 21–23°C), aliquoted, and quick-frozen in liquid nitrogen and stored at −70°C. On the day of use an aliquot was thawed (37°C) and spun. For experiments with IFM fibers, the protein was diluted with one-seventh volume of a relaxing buffer (250 mM imidazole; 73 mM EGTA; 51.2 mM $MgAc_2$; 47.2 mM ATP; 40 mM NaN_3; 120 mM CP; 415 mM potassium propionate; 160 μg/ml leupeptin; 800 units CPK and pH 7.0 at 21–23°C), resulting in a solution with the same composition as the μ = 195 mM relaxing solution in Table 1. For experiments with psoas fibers, the protein was mixed with one-seventh volume of a relaxing buffer (10 mM imidazole; 9 mM EGTA; 16.8 mM $MgAc_2$; 10.24 mM ATP; 40 mM CP; 1095 mM potassium propionate; 160 μg/ml leupeptin; 1600 units CPK), resulting in a solution with the same composition as the μ = 180 mM relaxing solution in Table 1.

TABLE 1 Solution composition

	Insect				Rabbit		
	Relaxing		Activating	Rigor	Relaxing	Activating	Rigor
Imidazole (mM)	40	40	40	40	10	10	10
K_2 EGTA (mM)	2	10	0	10	2	0	2
K_2 Ca-EGTA (mM)*	0	0	10	0	0	2	0
Magnesium acetate (mM)	3.6	6.4	6.3	1	2.1	2.1	0
Na_2ATP (mM)	3	5.9	6.0	0	1.28	1.28	0
Potassium propionate (mM)	0	0 (65)	0	30	30 (150)	150	160
NaN_3 (mM)	1	5	5	5	0	0	0
DTT (mM)	1	1	1	1	1	1	1
Na_2CP (mM)	2	15	15	0	5	5	0
CPK (units/ml)	100	100	100	0	200	200	0
Leupeptin (μg/ml)	20	20	20	20	20	20	20
pH (21–23°C)	6.8	6.8	6.8	6.8	7.0	7.0	7.0
μ (mM)†	45	130 (195)	130	90	60 (180)	180	180
pCa†	8.8	9.25	4.25	9.25	8.2	4.5	8.3
MgATP (mM)†	2.5	5	5	0	1	1	0
Mg^{2+} (mM)†	1.0	1.0	1.0	1.0	1	1	1

Abbreviations. CP, creatine phosphate; CPK, creatine phosphokinase.

* Obtained by mixing equimolar concentrations of EGTA and $CaCO_3$ and heating at 80°C until CO_2 production ceased (~10 min).

† Free and total concentrations were computed on an IBM AT computer using the program published by Fabiato (1988). The apparent binding constants and charges of the metal-ligand complexes were calculated for pH 6.8 at 22°C. Ionic strength, μ, was calculated from solution composition and the measured amount of KOH used to adjust pH. For pCa calculations a calcium contamination of 5 μM was assumed.

SDS gel electrophoresis

The protein composition of fiber fragments before and after FX-45 treatment was analyzed by SDS-polyacrylamide gel electrophoresis. A 3.1–12% gradient gel with a continuous buffer system of Fairbanks et al. (1971) was used for quantitating titin and nebulin (cf. Granzier and Wang, 1993b). A 3–18% acrylamide gradient and a 3% stacking gel of the Laemmli buffer system (Laemmli, 1970) was used for smaller proteins (Granzier, Wright, and Wang, manuscript in preparation).

Microscopy

The extent of actin removal was estimated by staining with 0.17 μM rhodamine-phalloidin (R-512; Molecular Probes, Eugene, OR) dissolved in relaxing solution. Fibers and myofibrils were fixed for 30 min in 3.7% (w/v) formaldehyde in relaxing solution, and then incubated with rhodamine-phalloidin for 2 h (IFM) or overnight (psoas). Fibers were transferred to microscope slides and covered with glass slips (No. 0; Thomson Scientific, Swedesburo, NJ) that were slightly elevated using 20-μm-thick gold grids. Fibers were scanned with a confocal microscope equipped with both phase and fluorescence optics (Zeiss Laser Scan Confocal Microscope; objective lens, 63 ×, 1.4 NA, Zeiss). Myofibrils were washed with relaxing solution and observed with a fluorescence microscope (Zeiss IM-35, objective, 100 ×, 1.25 NA; Zeiss, Thornwood, NY).

Muscle mechanics

Experiments were done with a computer-controlled workstation as described in Granzier and Wang (1993a). Briefly, a small (50 μl) quartz chamber was mounted on a XY-stage of an inverted microscope which contained also a servomotor (300S; Cambridge Technology Inc., Cambridge, MA) and a force transducer (AME 801E; Akers, Horton, Norway). The fiber was mounted using T-clips glued to the fiber ends. The clips were affixed to small hooks that were glued to the motor and the force-transducer. Solution in the chamber was exchanged by rapidly injecting new solution from an inlet at one end of the chamber and withdrawing it from the outlet positioned diagonally across the chamber. The solutions that were used are listed in Table 1. The chamber also contained a mixing port which was connected to a 10-μl syringe. This allowed a small volume of solution to be withdrawn from near the center of the fiber and then to be re-injected quickly for rapid mixing.

The chamber was mounted with its two long bottom corners inside two pipes that were cut open length-wise, to serve as air ducts. Studies at 5°C were done by circulating predried and precooled air around the chamber. The air was first sent through a copper coil surrounded by dry ice inside a box. The temperature of the solution inside the chamber could be lowered to 0°C, without noticeable airflow-induced vibration. Temperature was measured with a 75-μm wire thermocouple (J-type; Omega Engineering, Inc., Stamford, CT). The sensitivity of the force transducer varies with temperature, and the transducer was therefore calibrated at 5°C and 22°C.

For sarcomere length measurement, the fiber was illuminated by a He-Ne laser (106-2; Spectraphysics Analytical, San Jose, CA), to give rise to optical diffraction patterns. Sarcomere length was computed on-line, from the median position of either the first-order or second-order intensity profile, as described in Granzier et al. (1987). For most insect fibers, the diffraction patterns were sufficiently strong for detection at all degrees of stretch. Occasionally, however, fibers behaved differently: the diffraction pattern weakened initially to levels below the detection limit of the sensor, and then recovered at higher degrees of stretch, allowing sarcomere length to be measured again. The missing values were interpolated from the straight line of a fiber length versus sarcomere length plot. In all insect fibers, the diffraction pattern improved greatly following thin-filament removal, thus alleviating detection problems.

The diffraction patterns of rabbit fibers were strong and became more intense after thin-filament removal and no detection problems were encountered. For fibers that were highly stretched, sarcomere length was first calculated from the first-order diffraction peak, and when this peak had moved outside the photoactive area of the photodiode array, from the second-order position (Granzier et al., 1987). During the 10–30-s period needed to switch from first to second order, sarcomere length could not be measured, and these values were estimated by interpolation as described above for insect fibers.

The fibers were stretched with a constant velocity, that was selectable, to a predetermined amplitude and then released to its initial length. Each 350 ms of force, sarcomere length and tension were measured (8 μs per measurement). Concomitantly, the fiber was subjected to brief 15-ms bursts of high frequency sinusoidal length oscillations (2.2 kHz; amplitude 0.1%).

Each burst consisted of 32 oscillations (generated digitally). The ensuing tension oscillations were sampled, and the tension amplitude was determined, on-line, with FFT (fast Fourier transform) analysis. Stiffness was calculated as the ratio of the tension amplitude to strain amplitude. Stiffness was measured each 350 ms, thus allowing the time course of stiffness change to be monitored. Further details can be found elsewhere (Granzier and Wang, 1993a).

Mechanics protocol

Cross-sectional area of slack fibers were estimated by light microscopy as described in Granzier and Wang (1993a). The sarcomere length detector was calibrated and the sarcomere length of the central region of fibers was followed throughout the experiment. To ensure a stable slack length throughout the mechanical protocol, the fiber, and the clip-hook attachments were first exposed several times to the substantial forces that fibers develop in rigor solution (Granzier and Wang, 1993a). Subsequently, the fiber was kept in relaxing solution for 20 min, while the fiber was made to buckle slightly by moving the translators. The fiber was then stretched slowly and the length at which sarcomeres just started to elongate (measured on-line with laser diffraction) was taken as the slack length.

Mechanical properties of the fibers were characterized before and after FX-45 treatment. FX-45 (1 ml) was injected into the chamber using the normal solution exchange procedure. After 3-h incubation for IFM fibers or 7-h incubation for psoas fibers, the fiber was washed with relaxing solution (5 ml), and the mechanical properties were then measured again. The effect of the carboxyl-terminal caldesmon fragment on fiber mechanics was measured by incubating fibers in the presence of caldesmon for 2 h prior to mechanical measurements. To conserve material, caldesmon was added by withdrawing 10-μl solution from the chamber through the mixing port and replacing it with 10 μl of caldesmon solution. After mixing 10 times by withdrawing 10 μl of solution from the chamber and rapidly reinjecting the solution, this whole procedure was repeated again 15 times to bring the caldesmon concentration inside the chamber up to >95% of the added solution.

Passive tension and passive stiffness were measured by subjecting fibers to a continuous stretch to a predetermined amplitude followed by a continuous release with the same velocity. Previously we used protocols in which stretches and releases were periodically interrupted by long rest periods during which length was kept constant in order to allow stress relaxation to occur (Wang et al., 1991, 1993; Granzier and Wang, 1993a). In the present study, such periods of stress-relaxation were omitted. Ensuing passive tensions were identical to the peak tensions of the "old" protocol.

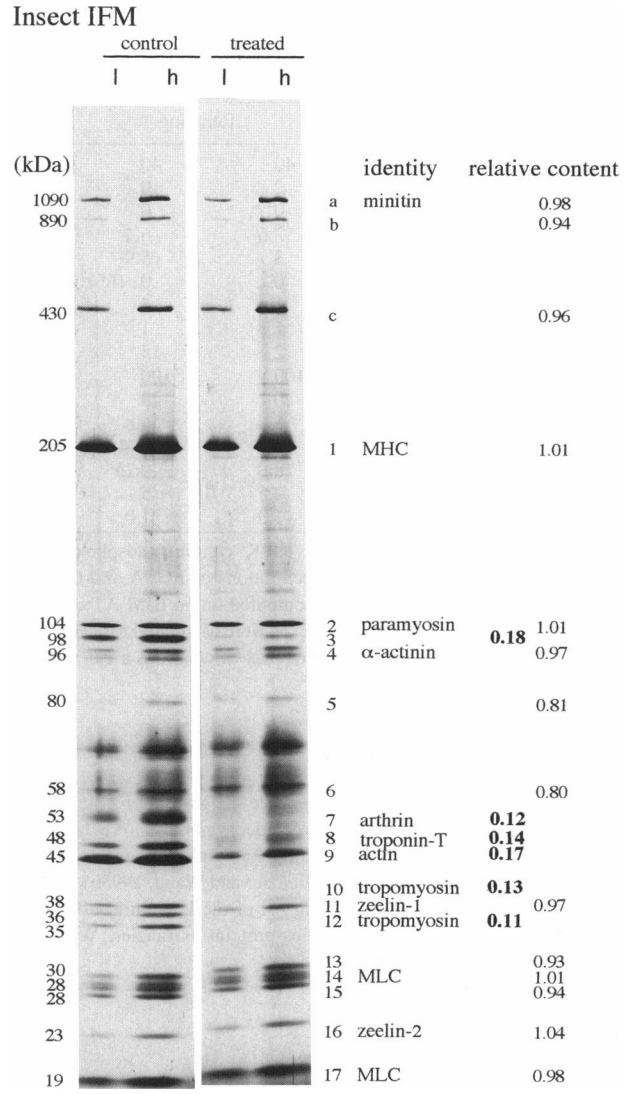

FIGURE 1 Effect of FX-45 treatment on protein composition of IFM fibers. Single fibers were solubilized, electrophoresed on a 3.8% Laemmli gel, and silver stained. "Control" lanes show an untreated fiber with a low (*l*) and high (*h*) loading corresponding to 0.3- and 0.8-mm fiber length. "Treated" lanes show a fiber after FX-45 treatment (7 h). Protein bands 3, 7, 8, 9, 10, and 12 were extracted by FX-45, as revealed by the reduction of relative protein content.

RESULTS

Effect of FX-45 on protein composition

Insect IFM

The rate of actin extraction was studied by incubating fibers with FX-45 in relaxing solution from 45 min to 7 h. The washed fibers were then analyzed with SDS-polyacrylamide gel electrophoresis. Fig. 1 shows an example of a fiber treated with FX-45 for 7 h. Actin and thin-filament based proteins such as arthrin, troponin-T, and tropomyosin were much reduced in intensity by the gelsolin treatment.

The degree of extraction was quantitated by loading various amounts of the same sample (expressed in millimeter fiber length) and determining the peak areas of protein bands as a function of loading. The level of extraction was then determined from the slopes of the *linear range* of the peak-area versus loading curve. Variations in slope due to differences in size of the fiber segments were normalized by expressing slopes relative to the slope of paramyosin that resisted extraction and was chosen as an internal standard. The relative extent of extraction of actin, arthrin, troponin-T, tropomyosin, and protein 3 were strikingly similar and all reached in 2–3 h a steady residual value of 0.1–0.2. Increasing incubation time to 7 h caused no additional extraction (Fig. 1).

Rabbit psoas

Similar studies on psoas fibers showed that FX-45 was equally effective. Fig. 2 shows a control fiber and a fiber treated for 9 h with FX-45 in relaxing solution. Actin, troponin-T (Tn-T), tropomyosin (Tm), and the doublet that

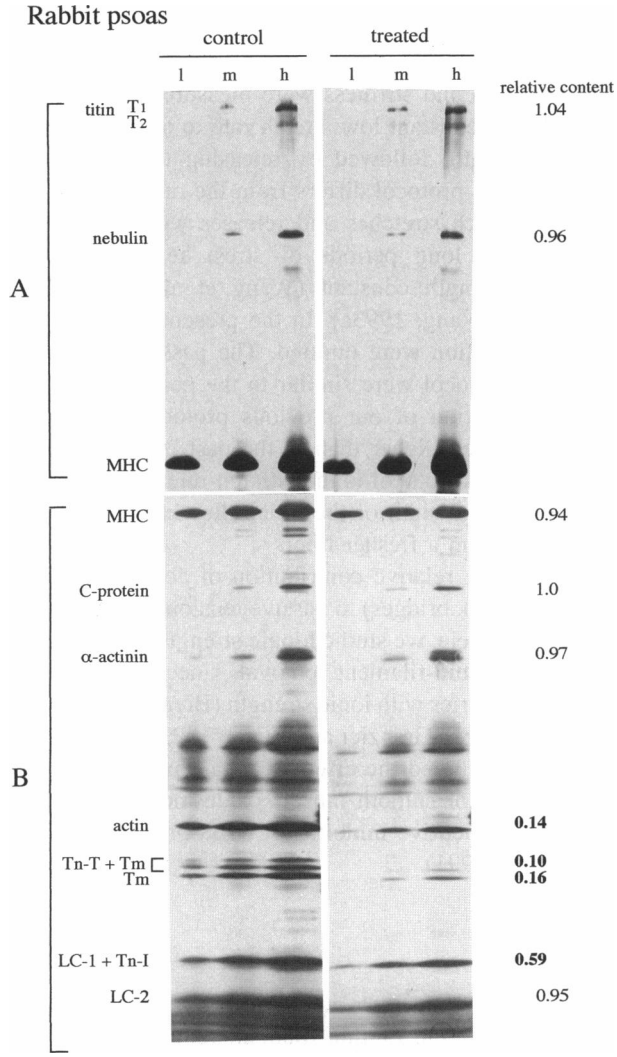

FIGURE 2 Effect of FX-45 treatment on protein composition of rabbit psoas fibers. Fibers were solubilized and electrophoresed on both a 3.1–12% Fairbanks gel (*A*) and a 3–18% Laemmli gel (*B*) and then silver-stained. "Control" lanes show an untreated fiber with a low (*l*), medium (*m*), and high (*h*) loading corresponding to 0.2-, 0.4-, and 1.2-mm fiber length, respectively. "Treated" lanes show a fiber after FX-45 treatment (9 h). Actin, troponin-T (*Tn-T*), and tropomyosin (*Tm*) were extracted.

likely consists of both light chain 1 and troponin-I (LC-1 + Tn-I) were extracted. The relative protein contents (normalized to C-protein content) of actin, troponin-T, and tropomyosin decreased in parallel with incubation time, until a residual value of 0.1–0.2 was reached in about 7 h, with no additional change upon further incubation (data not shown). The extraction rate appeared to be much slower than that of insect flight muscle.

Site and uniformity of actin removal

To locate the site of actin removal by FX-45 extraction, both fibers and myofibrils were treated and stained with rhodamine-phalloidin which binds F-actin. In both IFM and psoas myofibrils of untreated controls, phalloidin labeled the whole sarcomere more or less uniformly except for a narrow clear zone in the center of A band (H zone) and a more intensely stained Z-line region (Figs. 3 *A* and 4 *A*, controls). It was noted that uniform staining of thin filaments in rabbit psoas myofibrils was observed only after formaldehyde fixation (30 min) and overnight staining by phalloidin. Otherwise staining was nonuniform with distal ends of thin filaments and Z-line being more intense (cf. Wilson et al. 1987; Greaser and Schnasse, 1990). FX-45 treatment removed phase density in the overlap region without obvious effect on the Z-line (Figs. 3 *A* and 4 *A*, *phase, treated*). Phalloidin staining of treated myofibrils showed that actin outside the Z-line region was qualitatively removed by FX-45, while actin in the Z-line remained unextracted (Figs. 3 *A* and 4 *A*, *treated*).

Uniformity of actin extraction in single fibers was investigated by optically sectioning and through-fiber scanning of stained fibers with confocal microscopy. All sarcomeres in treated IFM and psoas fibers appeared uniformly extracted and no gradient of staining from the periphery to fiber core was observed (Figs. 3 *B* and 4 *B*). This demonstrated that thin-filament actin outside the Z-lines is completely and uniformly extracted.

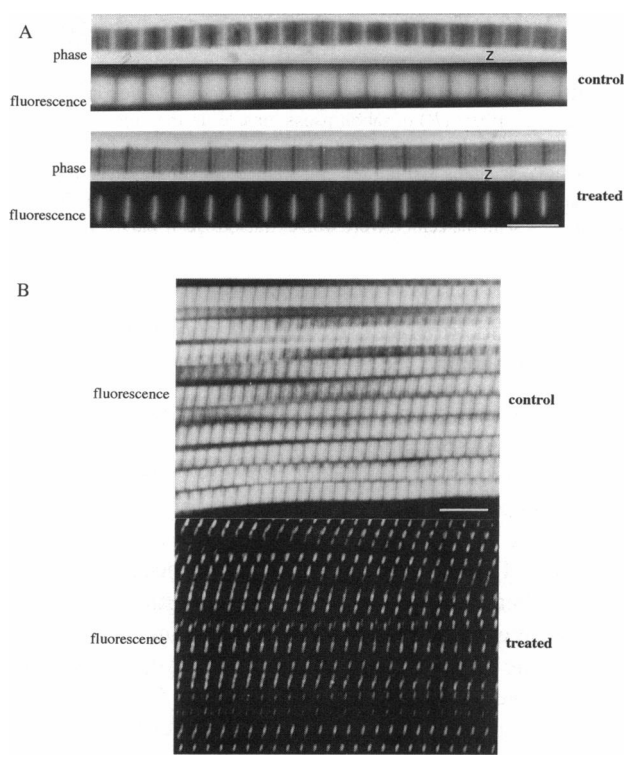

FIGURE 3 Effect of FX-45 treatment on actin distribution of myofibrils (*A*) and single fibers (*B*) of IFM. In untreated controls, actin staining was found throughout the sarcomere except for a narrow zone in the center (H zone). Elevated staining was observed at the Z-line region. After FX-45 treatment (7 h) only Z-line staining remained. In the fiber (*B*) all sarcomeres, including those in the center, were well extracted. Scale bars: 5 μm in *A* and 10 μm in *B*.

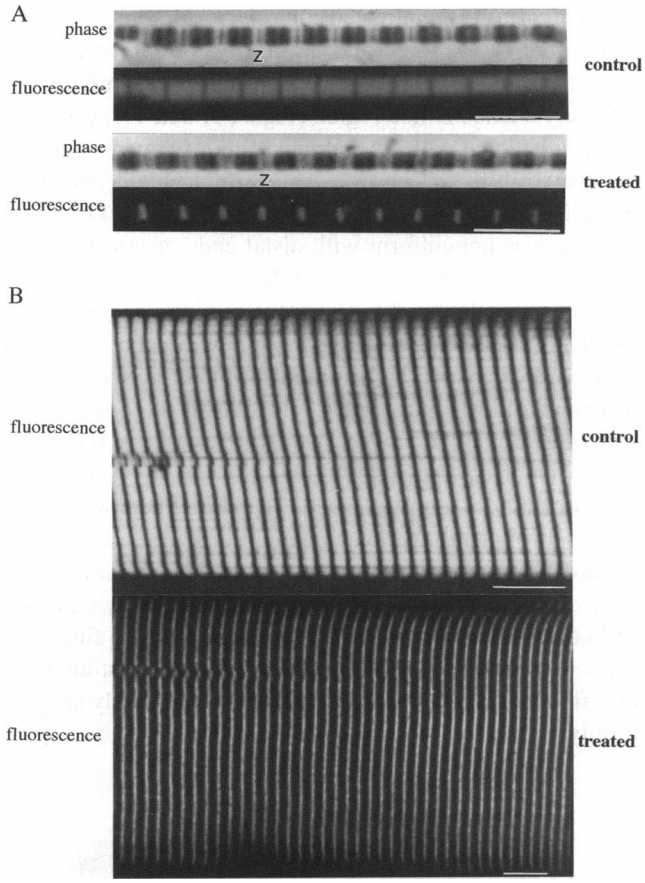

FIGURE 4 Effect of FX-45 treatment on actin distribution in myofibrils (*A*) and single fibers (*B*) of rabbit psoas muscle. In the untreated controls, actin staining was found throughout the sarcomere except in the H-zone. Z-lines and distal ends of thin filaments stained more intensely. After FX-45 treatment, only Z-line staining remained. All sarcomeres in the fiber (*B*), including those in the center, were well extracted. Scale bars: 5 μm in *A* and 10 μm in *B*.

Tension and stiffness of thin filament-free fibers in activating and rigor solutions

As an additional criterion for thin-filament removal, tension and stiffness during activation and rigor were measured before and after FX-45 treatment. For insect IFM, activation was accomplished by first stretching fibers in relaxing solutions (4% in 100 s) and activating after 2 min of stretch relaxation. The prestretch was necessary since active tension in IFM fibers is very low at the slack length and increases with passive tension at longer length (Granzier and Wang, 1993a). The fiber was then treated with FX-45 and the same protocols were repeated. As shown in Fig. 5 *A* and Table 2, all tension and stiffness values dropped below 5% of pretreatment levels. A similar reduction of tension and stiffness was observed for psoas fibers following thin-filament removal (Fig. 5 *B* and Table 2).

Since it is well established that tension and stiffness during activation and rigor predominantly arise from actomyosin interaction, these mechanical data confirmed the quantitative removal of thin filaments by FX-45 treatment.

Effect of thin-filament removal on passive tension and stiffness

Passive tension and stiffness were measured by stretching the fibers at a constant low stretch rate to a predetermined sarcomere length, followed by releasing the fiber at the same rate. This protocol differs from the one we used previously in which stretches and releases were periodically interrupted by long periods of stress relaxation, while keeping the length constant (Wang et al., 1991, 1993; Granzier and Wang, 1993a). In the present study, periods of stress-relaxation were omitted. The passive tensions of the current protocol were similar to the peak tension prior to stress-relaxation of our previous protocols, and fibers were not stressed higher than in the past. A major advantage of the new protocol is that stretch-release cycles were completed in one-sixth of the time, allowing more data to be collected from a fresher fiber.

To assess the relative contribution of actomyosin interaction (i.e., weak bridges) to passive tension and stiffness in the relaxed muscle, we studied ionic strength sensitivity before and after thin-filament removal, since the number of weak bridges varies with ionic strength (Brenner et al., 1982; Schoenberg, 1988; Granzier and Wang, 1993a). As a second approach, we studied the effect of a carboxyl-terminal (27 kDa) fragment of smooth muscle caldesmon, which functions as a competitive inhibitor of cross-bridge interaction (Wang et al., 1991).

IFM fibers

Passive tension was not much affected by either ionic strength, caldesmon, or thin-filament removal (Fig. 6 *A*). Typically, thin-filament removal resulted in only a slight drop in tension (Fig. 6 *A* and Table 2). Stiffness, on the other hand, was strongly depressed by thin-filament removal at all ionic strengths, with the greatest depression at μ = 45 mM, and the smallest at μ = 195 mM (Fig. 6 *B*). Interestingly, when control fibers were incubated with the caldesmon fragment at μ = 195 mM, stiffness was depressed to the same level as measured after thin-filament removal (Fig. 6 *B*). It appears thus that caldesmon completely inhibits weak bridge formation in insect IFM fibers in contrast to the partial inhibition by caldesmon (~75%) that has been reported for rabbit psoas fibers (Brenner et al., 1991). The effect of caldesmon was reversible in our study, since stiffness increased to the preincubation level when caldesmon was washed away.

In control fibers, plots of passive stiffness versus passive tension at the various ionic strengths could be fitted, above 10–20 kN m^{-2}, with a family of parallel straight lines with different stiffness intercept (Fig. 6 *C*). After actin removal, the plots remained linear with similar slopes but much reduced stiffness intercepts. Additionally, the relation was no longer sensitive to ionic strength. These data suggest that the high passive stiffness of IFM fibers can be

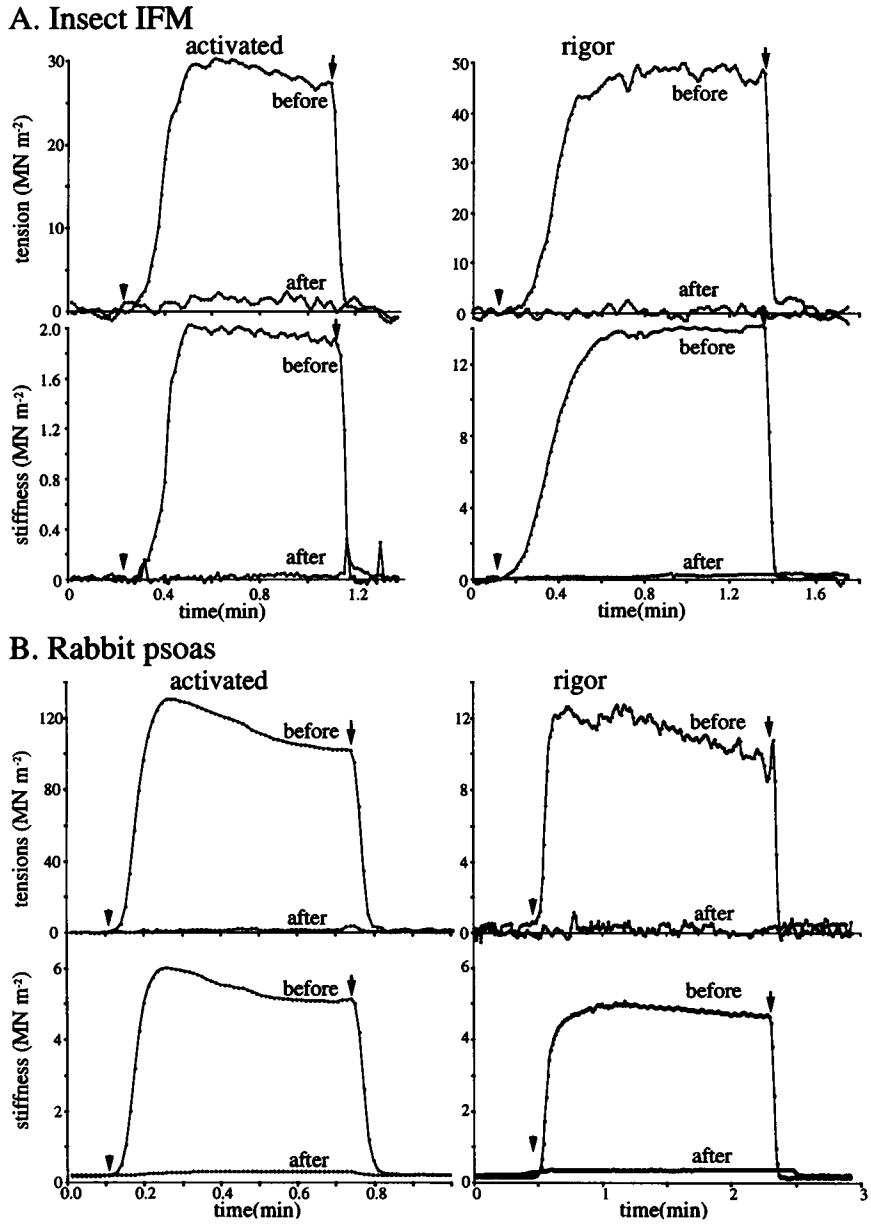

FIGURE 5 Effect of thin-filament removal on tension and stiffness of activated and rigor IFM (*A*) and psoas fibers (*B*). After thin-filament removal, tension and stiffness are greatly depressed (>95%). The arrowheads indicate switching to rigor or activating solution. Arrows indicate subsequent switching back to relaxing solution.

resolved into two components. One component is actin-based, since it is abolished by thin-filament removal. This component is likely to be derived from weak bridges, since it increases when ionic strength is lowered and is inhibited by the caldesmon fragment. Our results imply the existence of weak bridges in relaxing solution of μ = 195 mM and temperature of 21–23°C. The second stiffness component is neither affected by thin-filament removal nor by the presence of caldesmon. It is likely that this component is based on the C filament which in insect IFM fibers connects the end of the thick filaments to the Z-lines (Reedy, 1971). The linear relation between stiffness and tension of the C filaments implies that C filament elasticity is nonlinear (see also Granzier and Wang (1993a)).

Psoas fibers

For technical reasons, ionic strength studies were carried out at 22° and 5°C for the μ = 180 mM solution and at 5°C for the μ = 60 mM solution. We observed that when the μ = 60 mM solution was studied at 22°C, a large tension developed, and sarcomere length became inhomogeneous to the point that the blurred diffraction patterns were no longer suitable for sarcomere length measurement. (This phenomenon, also described by Brenner et al. (1982), was absent in IFM which could be studied in low ionic strength solution at 21–23°C.)

At these two temperatures, tension of control fibers did not vary substantially with ionic strength (Fig. 7 *A*). At all ionic strengths, plots of the natural logarithm (Ln) of tension

TABLE 2 Effect of thin filament removal on mechanical properties*

	IFM		psoas		Semitendinosus
	Control	Treated	Control	Treated	control
Slack length (μm)	2.68 ± 0.02	2.67 ± 0.04	2.00 ± 0.01	1.91 ± 0.03	2.12 ± 0.01
Active	(4% prestretch)‡		(10% prestretch)		
Tension (kN m^{-2})	28.0 ± 2.0	0.2 ± 0.2	110.2	0.5	
Stiffness (MN m^{-2})	1.7 ± 0.3	0.01 ± 0.02	5.5	0.1	
Rigor	(2% prestretch)‡		(10% prestretch)		(10% prestretch)
Tension (kN m^{-2})	28.1 ± 5.0	0.3 ± 0.2	8.7 ± 3.1	0.29 ± 0.1	7.3 ± 2.2
Stiffness (MN m^{-2})	11.3 ± 1.3	0.3 ± 0.1	5.5 ± 0.9	0.1 ± 0.1	6.2 ± 0.8
Passive					
E_0 (kN m)§	169 ± 43	215 ± 37	7.4 ± 1.4	11.7 ± 0.8	3.5 ± 2.0
α§	56 ± 8	47 ± 4	6.9 ± 0.1	6.8 ± 0.02	6.35 ± 0.21
Tension yield point (μm)	3.07 ± 0.01	3.06 ± 0.02	3.63 ± 0.03	3.60 ± 0.05	4.59 ± 0.09
Yield tension (kN m^{-2})	111 ± 10	90 ± 12.6	110 ± 7	148 ± 42	126 ± 10.0
Stiffness yield point (μm)	2.96 ± 0.04	2.93 ± 0.05	3.53 ± 0.07	3.53 ± 0.07	4.44 ± 0.09
Yield stiffness (MN m^{-2})	7.5 ± 0.8	4.5 ± 0.7	3.4 ± 0.5	1.9 ± 0.7	5.9 ± 1.4

* Measured at μ 195 mM for IFM fibers and μ 180 mM for psoas and semitendinosus fibers.

‡ Stretch prior to activation or rigor induction.

§ Passive tension (σ) – sarcomere strain (ϵ) relation fitted to: $\sigma = E_0\alpha^{-1}(e^{\alpha\epsilon} - 1)$.

versus sarcomere length were linear (except for lengths very close to the slack length), indicating that tension rose exponentially with sarcomere length (Fig. 7 *B*). This exponential rise can be described by the equation $\sigma = E_0\alpha(e^{-\alpha\epsilon} - 1)$ where σ = passive tension and ϵ = sarcomere strain (cf. Wang, et al. 1993). Thin-filament removal resulted in a slight (0.1 μm) reduction of slack sarcomere length and significantly higher tensions when sarcomeres were stretched (Fig. 7, *A* and *B*, and Table 2): the average increase in tension at 50% stretch was 72 ± 13%. Interestingly, the slope of the Ln tension versus sarcomere length plot was unaffected by thin-filament removal (Fig. 7 *B*), while the *Y*-intercept was higher, indicating that the exponent of exponential tension rise (α) was unchanged (Table 2).

Passive stiffness of control fibers varied greatly with ionic strength and temperature, e.g., it was higher by 1.7 MN m^{-2} (35% of rigor stiffness) at μ = 60 mM (5°C) than at μ = 180 mM (22°C) (Fig. 7 *C*). These findings suggest that a substantial number of weak bridges exist at low ionic strength and low temperature, in agreement with findings of others (Brenner et al., 1982; Schoenberg, 1988). Schoenberg (1988) reported that at high ionic strength (160 mM) and low temperature (5°C) about 7% of the cross-bridges are attached to actin. Whether weak bridges exist at 180 mM and a temperature of 22°C, however remained open. We investigated this question by measuring the effect of a carboxyl-terminal caldesmon fragment which inhibits actomyosin interaction. As shown in Fig. 8, passive tension was not affected much by caldesmon (Fig. 8 *A*) but passive stiffness was clearly depressed (Fig. 8 *B*). The level of depression, as determined from the differences in *Y*-intercepts of linear lines fitted through the stiffness-tension curves in Fig. 8 *C*, was found to correspond to 0.13 MN m^{-2}, or 4.6% of rigor stiffness. We conclude that weak bridges do exist, in modest numbers, in psoas fibers under physiological conditions (μ = 180 mM; 22°C).

The relative contribution of weak bridges and titin to passive stiffness was analyzed by plotting passive stiffness versus passive tension. As shown in Figs. 7 *D* and 8 *C*, curves above 10 kN m^{-2} were linear with similar slopes ($r^2 > 0.99$) but different *Y*-intercepts. In the presence of caldesmon or after actin removal, the plots remain linear with the same slope, but with a much reduced stiffness intercept. Most importantly, the relation was no longer sensitive to ionic strength. Thus the stiffness–tension curves can be resolved into two components: a weak bridge component that is ionic strength and caldesmon-sensitive and is abolished by actin removal, and a titin component that is insensitive to ionic strength, caldesmon, and actin removal. Our findings indicate that weak bridge stiffness does not vary with passive tension and that, in contrast, titin stiffness increases linearly with passive tension.

The conclusion that weak bridge stiffness is independent of tension is unexpected since it implies that this stiffness does not vary much over the sarcomere length range of ~2.5–3.0 μm, where curves are linear (Fig. 7 *D*). This is contrary to the report by Brenner et al. (1982) that showed that weak bridge stiffness of psoas fibers decreases linearly with sarcomere length. To explore this further, we extended our measurements over a wider range of sarcomere length and used the same solution compositions as reported in Brenner et al. (1982) to allow a closer comparison.

Passive tension and stiffness were measured at μ = 20 mM and μ = 170 mM at sarcomere lengths ranging from 2.1 to 3.5 μm according to the protocol in Fig. 9 *A*. Fibers were stretched by 10% in 100 s and then held constant for 260 s. This was repeated until 80% stretch was reached. The fiber was then released (10% in 100 s, followed by 260 s of rest) until the original slack length was attained. The stretch-release cycle was repeated after a 40-min rest period.

Passive tensions at μ = 20 mM and μ = 170 mM were found to be similar, but stiffness was significantly different. Fig. 9 *B* shows the stiffness reached at the end of each 10%

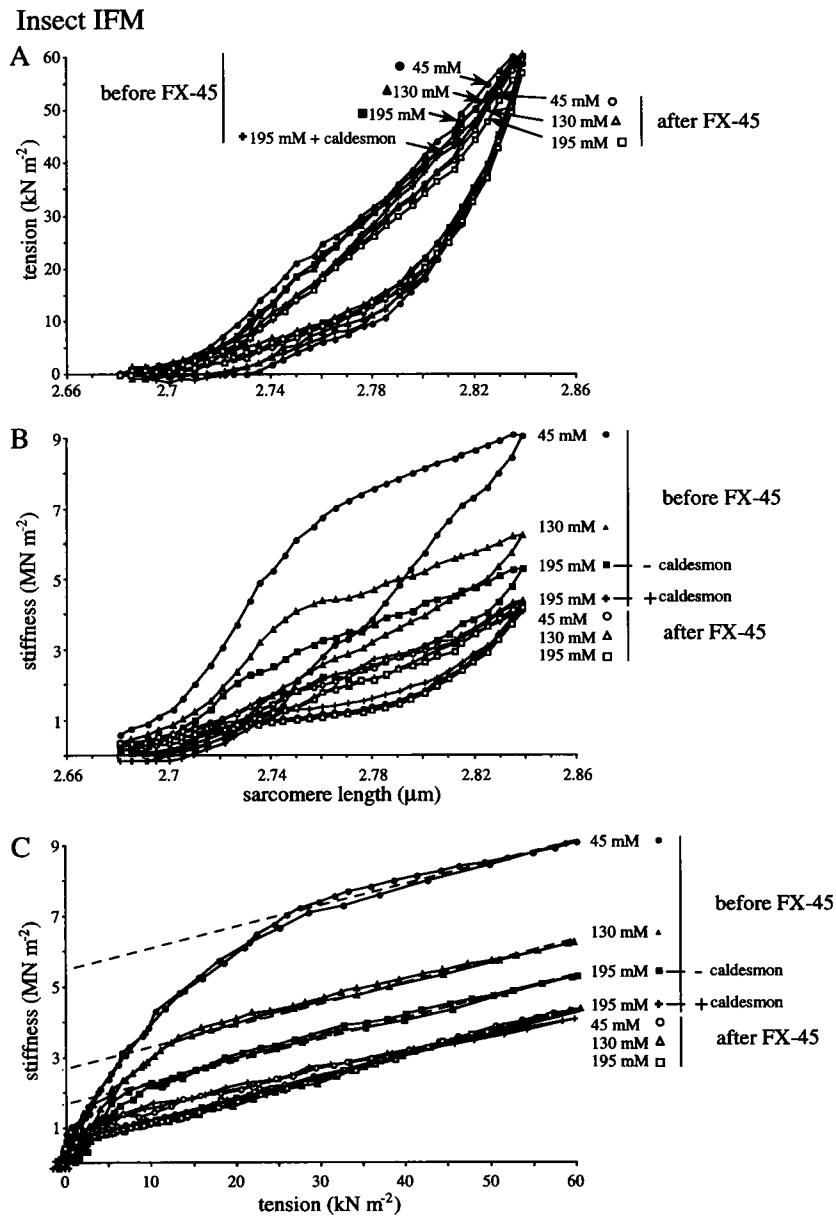

FIGURE 6 Effect of thin-filament removal on tension and stiffness of a passive IFM fiber. The fiber was stretched at a constant rate (6% in 180 s) and then released with identical rate. Fiber length, sarcomere length, and tension and stiffness were measured every 350 ms. This protocol was carried out on the untreated fiber in relaxing solutions of three ionic strengths (μ): 45, 130, and 195 mM, followed by the addition of caldesmon fragment (μ = 195 mM) and then in relaxing solution (of μ = 45, 130, and 195 mM), after thin-filament removal with FX-45. (*A*) Passive tension-sarcomere length plots. Passive tension did not vary significantly with ionic strength and was not affected by caldesmon. (*B*) Passive stiffness-sarcomere length plots. Prior to thin-filament removal, stiffness increased with decreasing ionic strength. Thin-filament removal also abolished the ionic strength sensitivity of stiffness. Addition of caldesmon at μ = 195 mM before thin-filament removal resulted in a reduction of stiffness to the same level as that measured after thin-filament removal. (*C*) Passive stiffness-tension plots. For tensions higher than 10–20 kN m^{-2}, stiffness varied linearly with tension. In the control curves, the linear portion of the stiffness-tension plot at the different ionic strengths had similar slopes, but were shifted along the stiffness axis (45 mM: $Y = 0.059X + 5.9$; 130 mM: $Y = 0.053X + 3.05$; 195 mM: $Y = 0.057X + 1.92$). Thin-filament removal did not affect the slope, but shifted the linear curve down the stiffness axis (45 mM: $Y = 0.059X + 0.7$; 130 mM: $Y = 0.067X + 0.4$; 195 mM: $Y = 0.065X + 0.4$). Addition of caldesmon at μ 195 mM resulted in a stiffness-tension plot that was similar to that measured after thin-filament removal ($Y = 0.052X + 1.0$).

stretch/release (*closed symbols*) and at the end of the 260-s rest period (*open symbols*). In Fig. 9 *C* the differences between the stiffness values at μ = 20 mM and μ = 170 mM (ΔE) were plotted to represent weak bridge stiffness as a function of sarcomere length.

As sarcomeres were stretched from the slack length, weak bridge stiffness (ΔE) increased more than 50%, reached a maximum at 2.5 μm and then decreased with further stretch (*solid lines*, Fig. 9 *C*). The decrease, however, was less than that predicted from the assumption that stiffness decreases linearly with the degree of filament overlap (as indicated by the *solid straight line* in Fig. 9 *C*). For example, at 3.0 μm, ΔE measured at the end of each stretch (*solid lines*) was 93% of the maximum, whereas filament overlap had dropped to 56% of the maximum. At longer sarcomere lengths (>3.2 μm), however, ΔE decreased faster than filament overlap and finally extrapolated to zero at about 3.8 μm, where filament overlap is zero (Fig. 9 *C*). The modest drop (7%) in ΔE from 2.5 to 3.0 μm supports the conclusion drawn from Figs. 7 *D* and 8 *C* that weak bridge stiffness does not vary much with filament overlap over this range.

As sarcomeres were released from 3.5 μm, ΔE at a given sarcomere length was much less than during stretch. For example, ΔE at 2.5 μm after release was only 50% of that after stretch. A new theoretical curve was determined for the lower ΔE values after release (*dotted straight line*, Fig. 9 *C*), and it is interesting that ΔE measured after release is relatively close to the expected values based on filament overlap.

Passive tension-sarcomere length relations

IFM fibers

The recently proposed segmental-extension model of passive tension development (Wang et al., 1991, 1993) was tested on

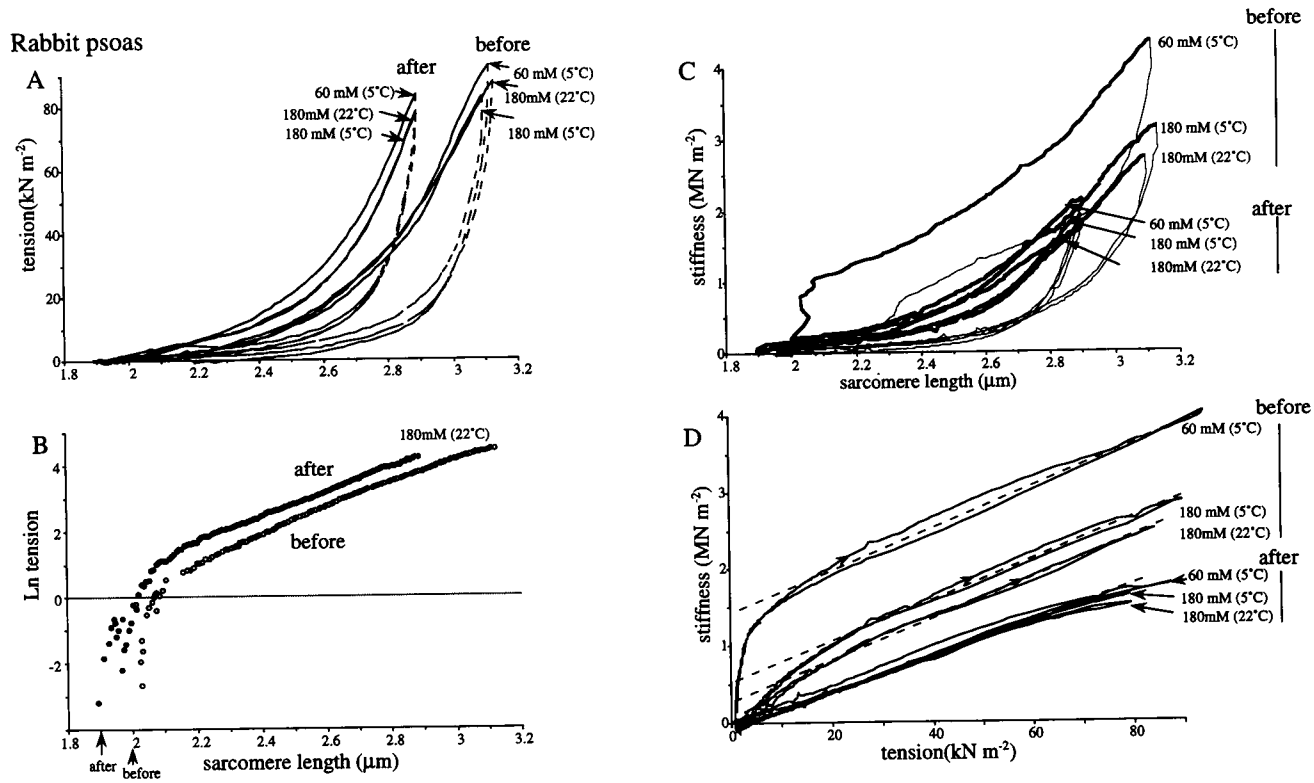

FIGURE 7 Effect of thin-filament removal on passive tension and stiffness of a rabbit psoas fiber. The fiber was stretched at a constant rate by 60% in 180 s and was then released with identical rate. Fiber length, sarcomere length, tension, and stiffness were measured every 350 ms. This protocol was carried out in different relaxing solutions in the following order: 180 mM (22°C), 180 mM (5°C), 60 mM (5°C), FX-45 treatment for 7 h (22°C), 180 mM (22°C), 180 mM (5°C), and 60 mM (5°C). Since the sarcomere slack length decreased from 2.0 to 1.9 μm during FX-45 treatment, the stretch protocol started from 1.9 μm in "after" curves. (*A*) Passive tension-sarcomere length plots. For a given sarcomere length, passive tension was significantly higher after thin-filament removal. (*B*) Natural logarithm of tension versus sarcomere length before and after thin-filament removal. The slopes of the lines above 2.2 μm are very similar. (*C*) Stiffness-sarcomere length plots. In the control cycles, stiffness increased with decreasing ionic strength. Ionic strength sensitivity was largely abolished by thin-filament removal. (*D*) Stiffness-tension plots. For tensions higher than about 10 kN m^{-2}, stiffness varied linearly with tension ($r^2 > 0.98$ for all curves). In the control curves, the linear portion of the stiffness-tension plots at the different ionic strengths had similar slopes but were shifted along the stiffness axis (60 mM: $Y = 0.025X + 1.79$; 180 mM 5°C: $Y = 0.027X + 0.76$; 180 mM 22°C: $Y = 0.028X + 0.41$). Thin-filament removal did not affect the slope, but shifted the linear relation further down the stiffness axis (60 mM: $Y = 0.024X + 0.04$; 180 mM 5°C: $Y = 0.024X + 0.01$; 180 mM 22°C: $Y = 0.023X + 0.001$).

thin filament-free fibers. Fibers in relaxing solution were stretched to a predetermined amplitude and then released with the same velocity back to the initial length. Each cycle of stretch and release was followed by a 40-min rest period. Fig. 10 shows the behavior of a thin filament-free IFM fiber, subjected to three cycles of stretch and release with stretch amplitudes of 15, 30, and 50% of the initial length, respectively. Passive tension of cycle 1 increased steeply with stretch and approached a plateau value (yield point) at 3.03 μm (Fig. 10 *A*). Slack length at the start of the second cycle was longer (from 2.68 to 2.70 μm), while the slope of the tension-length curve was depressed. Tension reached a maximum in cycle 2 that was similar to that of cycle 1 but the yield point was found at a longer sarcomere length (3.15 μm in cycle 2 versus 3.03 μm in cycle 1). In cycle 3 the increase in slack sarcomere length, the decrease in slope of the tension versus sarcomere length curve, and the decrease in yield point became more pronounced (slack length at 2.75 μm and yield point at 3.40 μm).

Tensions were also plotted versus *I* segment extension ratio. *I* segment length was estimated as the distance between A band and Z-line and segmental extension was expressed as an *I* segment length ratio. For cycle 1, *I* segment length of slack sarcomeres was taken as 0.05 μm (White, 1983), and the *I* band extension during stretch as half of the increase in sarcomere length. For cycles 2 and 3, the increase in slack sarcomere length was assumed to result from an increase of *I* band width, resulting in an initial *I* segment length of 0.06 μm for cycle 2 and 0.085 μm for cycle 3. When tension was plotted versus *I* segment extension ratio for each cycle, stretch curves below about 2.5 μm of the three cycles were nearly superimposable (Fig. 10 *B*), indicating that extension of the *I* segment of the C filament is sufficient to explain the initial shape of the passive tension-length curve.

Passive stiffness increased steeply with sarcomere length, reached a maximum, and then declined with further stretch (Fig. 10 *C*). Slopes of stiffness-length relations of subsequent loops were reduced, as were the maximal stiffness values at the yield point (Fig. 10 *C*). When stiffness was plotted against the *I* segment extension ratio, the slopes of the three stretch cycles were much closer (Fig. 10 *D*). Additionally,

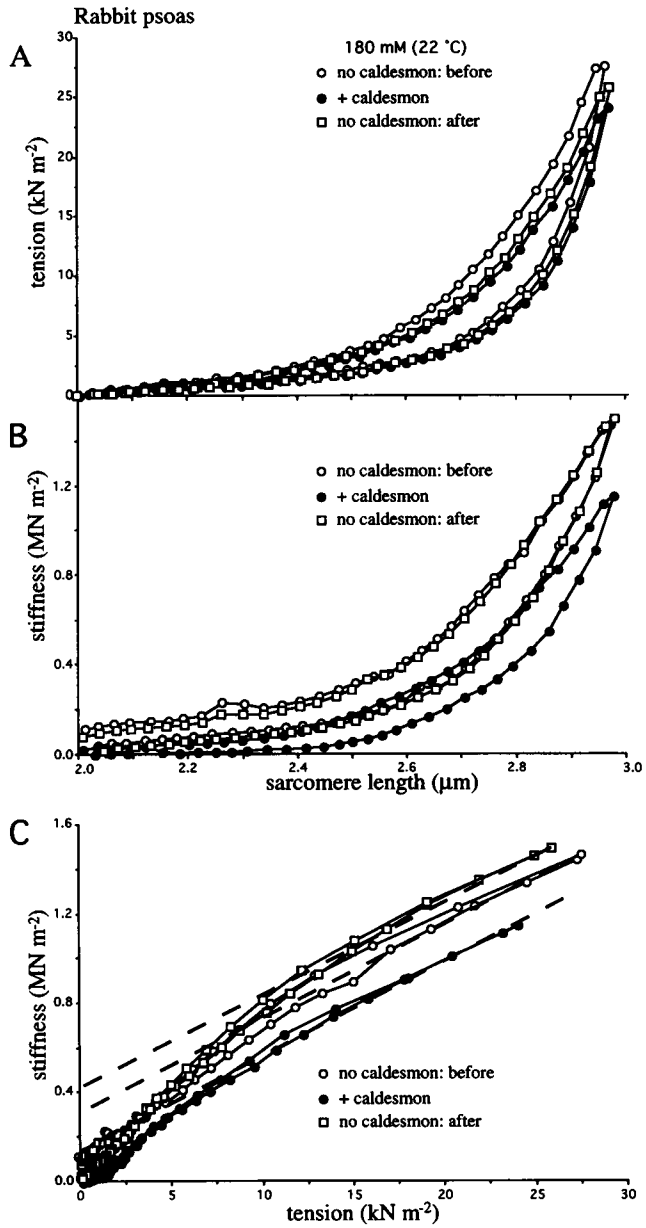

FIGURE 8 Effect of caldesmon on passive tension and stiffness of rabbit psoas fiber in relaxing solution at μ = 180 mM and 22°C. The fiber at slack length was stretched by 50% in 3 min and then released with the same rate back to the initial length. The stretch-release protocol was repeated after the fiber had been incubated with caldesmon fragment (2 mg/ml) for 2 h and again after 15 min of washing with relaxing solution (5 ml). (*A*) Passive tension–sarcomere length plots. Passive tension was not much affected by caldesmon. (*B*) Stiffness–sarcomere length plots. Stiffness was depressed by caldesmon, both during the stretch and release curves of the cycle. (*C*) Passive tension–passive stiffness plots. For tensions higher than about 10 kN m^{-2}, stiffness varied linearly with tension both in the absence and in the presence of caldesmon ($r^2 > 0.98$). The slopes of the linear regression lines were similar, while the *Y*-intercept was reduced in the presence of caldesmon. The reduction was 0.13 MN m^{-2} or 4.6% of rigor stiffness of this fiber (2.85 MN m^{-2}).

the stiffness yield-point for all cycles now appeared around an *I* segment extension ratio of 3 (Fig. 10 *D*). The maximal stiffness, however, still differed for the three cycles. In view of the fact that stiffness was measured with a high frequency sinusoid of constant amplitude (0.1% of the original slack length of cycle 1), the relative amplitude of imposed oscillation of the extensible *I* segment in cycles 2 and 3 are smaller by a factor 1.2 for cycle 2 and 1.7 for cycle 3, due to the increase in *I* segment length. By making the assumption that the amplitude of oscillation and stiffness are linearly related, we normalized the stiffness of cycles 2 and 3 by multiplying measured stiffness values of cycles 2 and 3 by 1.2 and 1.7, respectively. Remarkably, this additional normalization procedure merged all three cycles into a single amplitude-normalized stiffness versus *I* segment extension ratio plot, with nearly identical slope, maximal stiffness and yield point (Fig. 10 *E*).

Psoas fibers

Similar experiments were also carried out on thin-filament free psoas fibers. In the example shown in Fig. 11, the fiber was stretched by 60% in 3 min to 2.85 μm, well below the yield point, and then released back to the slack length (stretch 1). After a 40-min rest period, the fiber was stretched to 4.0 μm with the same velocity (stretch 2). Tension rise of the second stretch overlapped with that of the first loop, reached a plateau at the yield point of 3.63 μm, and remained constant with further stretch until the fiber broke (Fig. 11 *A*). Stiffness rise of the first and second stretch also overlapped, while stiffness of stretch 2 reached a maximum at a sarcomere length of 3.50 μm. Further stretch resulted in a 0.2 MN m^{-2} decline of stiffness (8% of the peak value) until the fiber broke. When stiffness was plotted versus tension, a biphasic linear relation was obtained, with a decrease in slope above a tension of 80 kN m^{-2} (Fig. 11 *C*). These data confirm and extend our previous observations that the yield-point phenomena is independent of thin-filament length (Wang et al., 1993). Additionally, as is the case with IFM fibers, the stiffness yield-point occurs at a shorter sarcomere length than the tension yield point.

I segment strain rate and passive tension and passive stiffness

We further tested the segmental extension concept of passive tension development by carrying out a comparative study of both tension and stiffness of fibers with different *I* segment length, with pro-tocols that result in the same *I* segment strain in the different fibers. IFM fibers and rabbit psoas fibers and rabbit semitendinosus fibers were selected, since these muscles express different size variants of titin and thus possess different *I* segment lengths (Wang et al., 1991, 1993). The imposed stretch rates on the fibers were such that the *I* segment strain rates were the same for these different fibers.

Special attention was also given to the manner with which to determine the slack sarcomere length, since the slack *I* segment length (I_0) depends critically on this value. For this purpose, fibers were shortened until they clearly

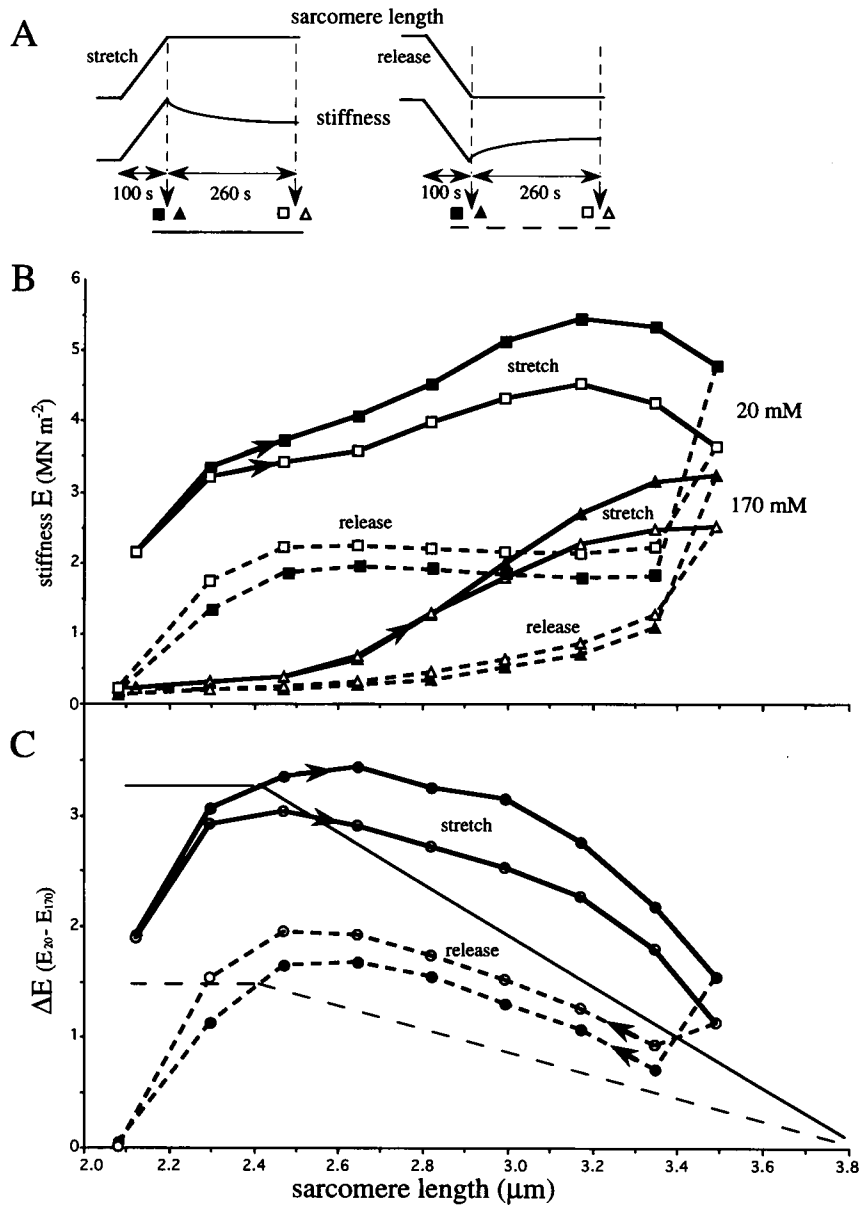

FIGURE 9 Sarcomere length dependence of weak bridge stiffness. (*A*) Protocol. The fiber was stretched 10% in 100 s followed by a 260-s relaxation period. The fiber was then stretched again. Release was done in a similar fashion. Stiffness was measured each 350 ms. (*B*) Stiffness-sarcomere length plot measured at 5°C in relaxing solution with μ = 20 mM and μ = 170 mM. Stiffness values at the end of stretch or release (*closed symbols*) and at the end of relaxation (*open symbols*) were plotted. Stiffness is much higher at μ 20 mM. (*C*) Stiffness difference (between low and high ionic strength, ΔE) = sarcomere length plot. ΔE is significantly higher during stretch (*solid lines*) than during release (*dotted lines*). ΔE displays a maximum at about 2.5 μm and then decreases modestly with sarcomere stretch. All ΔE curves deviated from the predicted stiffness values based on the assumption that stiffness decreases linearly with filament overlap (*straight lines*). The solid straight line assumes that ΔE at 2.4 μm where overlap is maximal, is 3.5 MN m^{-2} (maximal ΔE from measurements at end of each 10% stretch) the broken line assumes that ΔE at 2.4 μm is 1.5 MN m^{-2} (maximal ΔE from measurements at end of each 10% shortening). Rigor stiffness of this fiber was 6 MN m^{-2}.

buckled and were kept in this state for 20 min. The fibers were then stretched slowly and the length at which sarcomeres just started to elongate (measured on-line with laser diffraction) was taken as the slack length. The *I* segment length in slack sarcomeres (I_0) of rabbit fibers was calculated by subtracting half of the thick filament length (0.8 μm) from the half sarcomere slack length (cf. Wang et al., 1993), resulting in an I_0 of 0.20 and 0.26 μm for psoas and semitendinosus, respectively. Since the exact thick filament length of IFM fibers is not known, we assumed that I_0 was 0.05 μm, which is the same as the *I* band width at the slack length (White, 1983). The *I* segment stretch rate was chosen as 300% I_0 in 180 s, and the sarcomere stretch rate calculated accordingly.

Fig. 12 shows the tension and stiffness curves measured with this constant segment-strain-rate protocol. Tension of all fibers rose with sarcomere length in an exponential fashion, and the first parts of all curves could be fitted well ($r^2 > 0.98$) to an exponential equation (see Table 2) with a similar exponent (α) for psoas and semitendinosus fibers, but a much higher value for IFM fibers (Table 2). All fibers also showed a tension plateau. The plateau was maintained in the IFM fiber until the preparation broke, whereas the plateau in the rabbit fibers was followed by a second phase of tension rise. It has been shown that this second tension rise results from the extension of intermediate filaments at high sarcomere lengths (Wang et al., 1993). The absence of a significant second tension rise in IFM fibers thus implies that intermediate filaments are either absent or not involved in passive tension development. This conclusion is in agreement with the absence of substantial tension development by fibers that were treated with 1 M KI (Fig. 12) to remove thin and thick filaments but keep the intermediate filament system functional

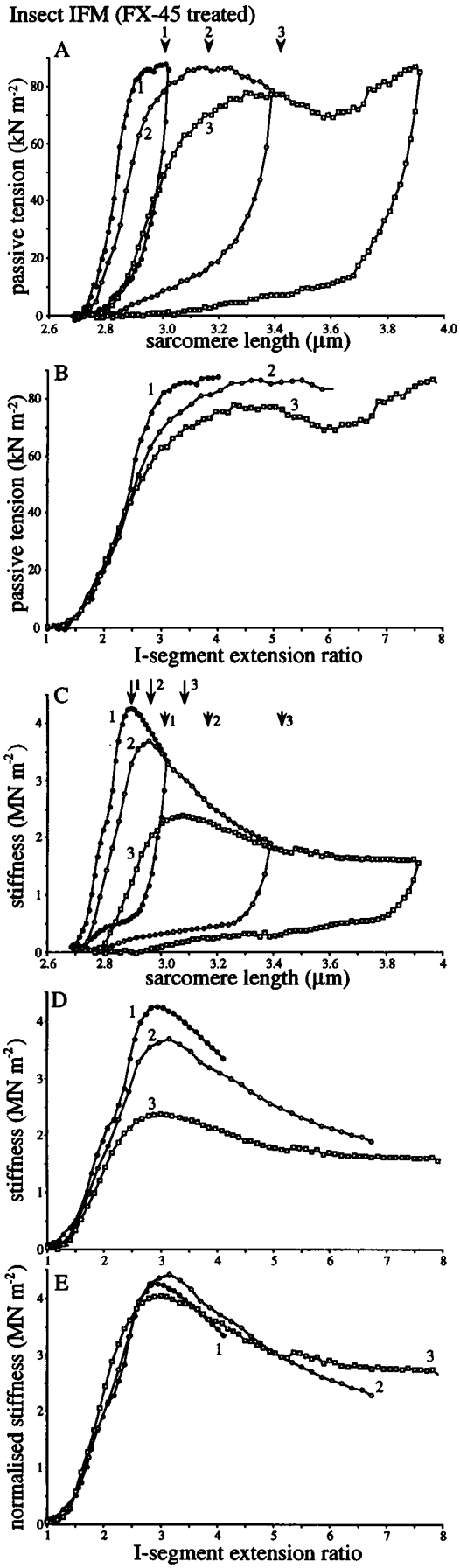

FIGURE 10 Passive tension and stiffness of thin filament-free IFM fiber. The FX-45 treated fiber in relaxing solution (μ = 195 mM) was stretched continuously with a rate of 5% per 3 min to a predetermined sarcomere length and then released with the same rate back to the initial sarcomere length. (*A*) Passive tension–sarcomere length plots. (*B*) Passive tension–*I* segment extension plots. (*C*) Passive stiffness–sarcomere length plots. (*D*) Passive stiffness–*I* segment extension ratio plots. (E) Normalized stiffness *I* segment extension ratio plots. Arrowheads indicate tension yield points, arrows indicate stiffness yield points. See text p. 2150 for further details.

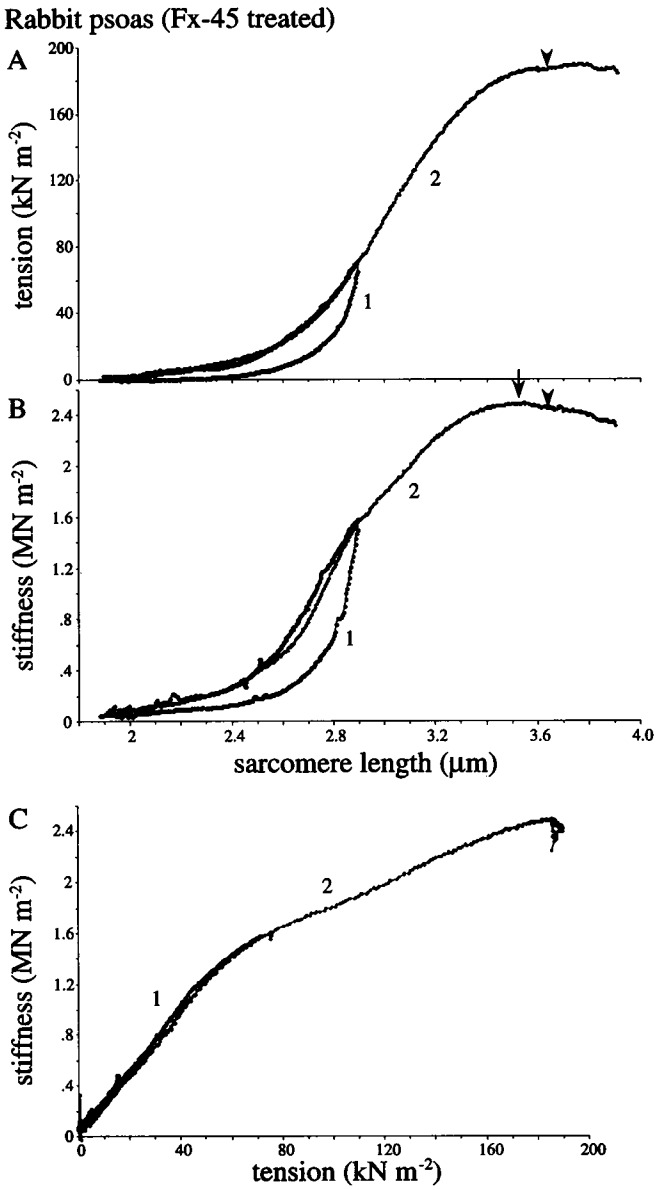

FIGURE 11 Passive tension and passive stiffness of thin filament-free psoas fiber. The fiber in relaxing solution (μ = 180 mM), was stretched continuously with a rate of 60% per 3 min to a predetermined sarcomere length and was then released with the same rate back to the initial length. The first stretch-release cycle (60% stretch) is followed by stretch until the fiber broke. (*A*) Passive tension–sarcomere length plot. (*B*) Passive stiffness–sarcomere length plot. (*C*). Passive stiffness–tension plot. See text p. 2151 for further details.

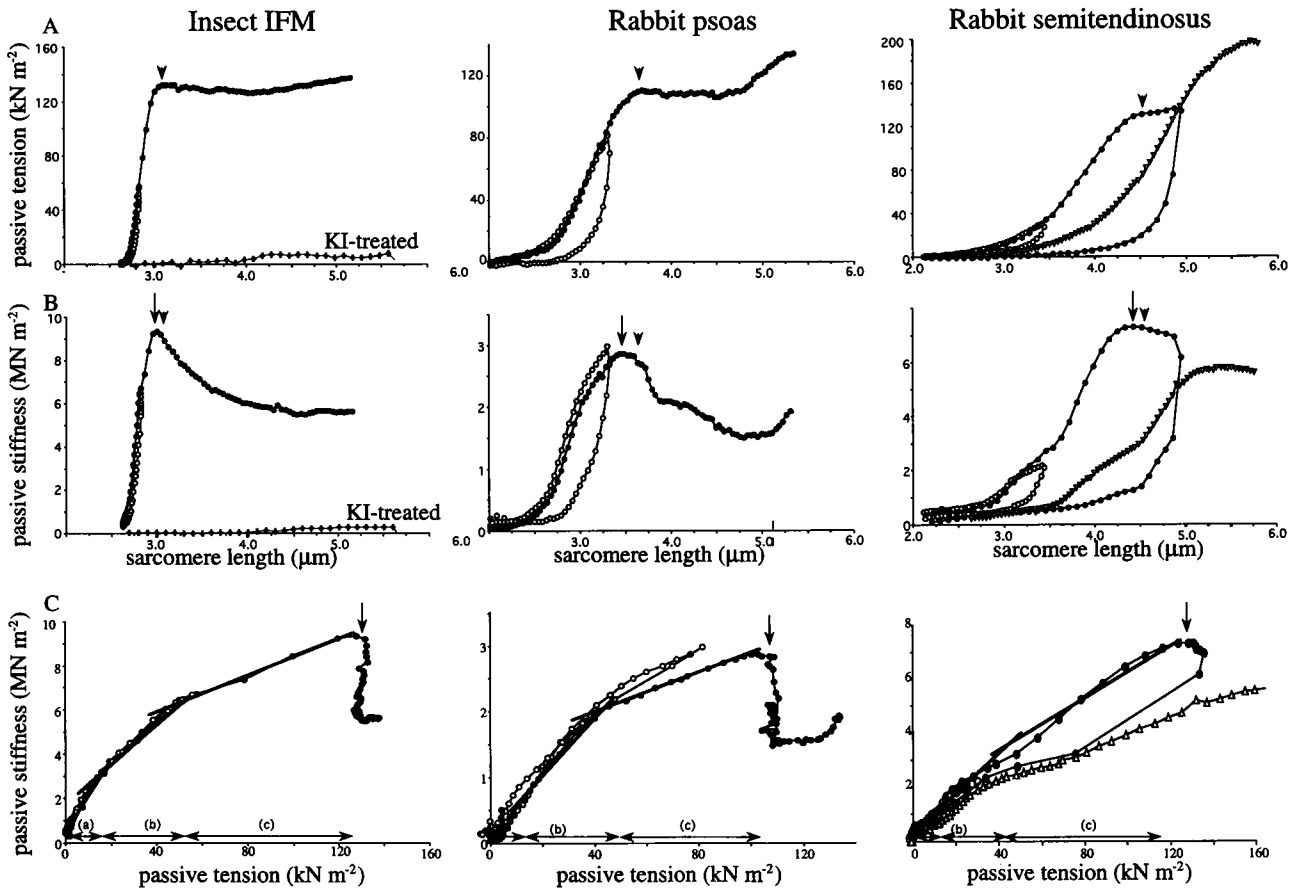

FIGURE 12 *A* and *B* Passive tension versus sarcomere length (*A*) and passive stiffness versus sarcomere length (*B*) obtained with a constant *I* segment stretch rate of 300%/180 s for all three muscle types. Imposed sarcomere stretch rates were 11%/3 min for IFM, 60%/3 min for psoas, and 75%/3 min for semitendinosus. When multiple stretch-release cycles were performed, a 40-min rest period in between cycles was allowed. IFM fiber (μ = 195 mM) was first stretched by 5%, released to the slack length and then stretched continuously until the fiber broke at a sarcomere length of 5.15 μm. Tension rose steeply until a plateau was reached at 3.07 μm that was maintained until breakage occurred (*A*). Stiffness reached a maximal value at 3.02 μm and decreased with further stretch (*B*). In a parallel experiment a different segment of the same IFM fiber was treated with 1 M KI in relaxing solution for 10 min prior to stretch (KI in *A* and *B*). The psoas fiber (μ = 180 mM) was first stretched by 60%, released and then stretched again until the fiber broke at 5.5 μm. Tension reached a maximum at 3.65 μm and then stayed constant until 4.8 μm was reached after which tension started to increase again (*A*). Stiffness reached a maximum at 3.50 μm, declined and increased again at 4.9 μm. The semitendinosus fiber (μ = 180 mM) was first stretched to 75% and released, then stretched to 150% and released, and finally stretched until the fiber broke at 5.8 μm. The second stretch-release cycle (*solid circles*) displayed a maximum in tension at 4.55 μm (*A*) and in stiffness at 4.45 μm (*B*). Stiffness declined with further stretch, while tension maintained a plateau (*B*). Tension and stiffness rose less steeply in the last stretch-release cycle (*triangles*). (*C*) Passive stiffness versus passive tension plots. (*a–c*) Various zones in the curves that can be distinguished. See text for further details. Arrowhead, tension yield point; arrows, stiffness yield point.

(White, 1983; Wang and Ramirez-Mitchell, 1983). It is worth noting that stiffness again peaked before tension did (Fig. 12 and Table 2) and that stiffness subsequently declined while tension was either still rising or constant.

To determine whether the tensions obtained with the constant *I* segment strain protocol correlate better with the degree of extension of either the sarcomeres or the *I* segment, we plotted tension versus sarcomere extension ratios (Fig. 13 *A*) and *I* segment extension ratios (Fig. 13 *B*). It is clear that only the *I* segment extension ratio, not sarcomere extension ratio, results in nearly overlapping tension curves, indicating that the *I* segment is a major determinant of passive tension development.

DISCUSSION

Selective actin filament extraction in the absence of calcium by a cloned gelsolin fragment

Full length gelsolin purified from plasma has been proven useful in the selective extraction of actin filaments from striated muscle (Funatsu et al., 1990; Kruger et al., 1991; Granzier and Wang, 1993a). To satisfy the calcium requirement of gelsolin, fibers in those studies were incubated in 0.1 mM Ca^{2+} for many hours (Funatsu et al., 1990). It has been observed that following such long-term calcium exposure of rabbit psoas fibers, nebulin is partially degraded (Funatsu et al., 1990), while Z-line densities tend to be reduced

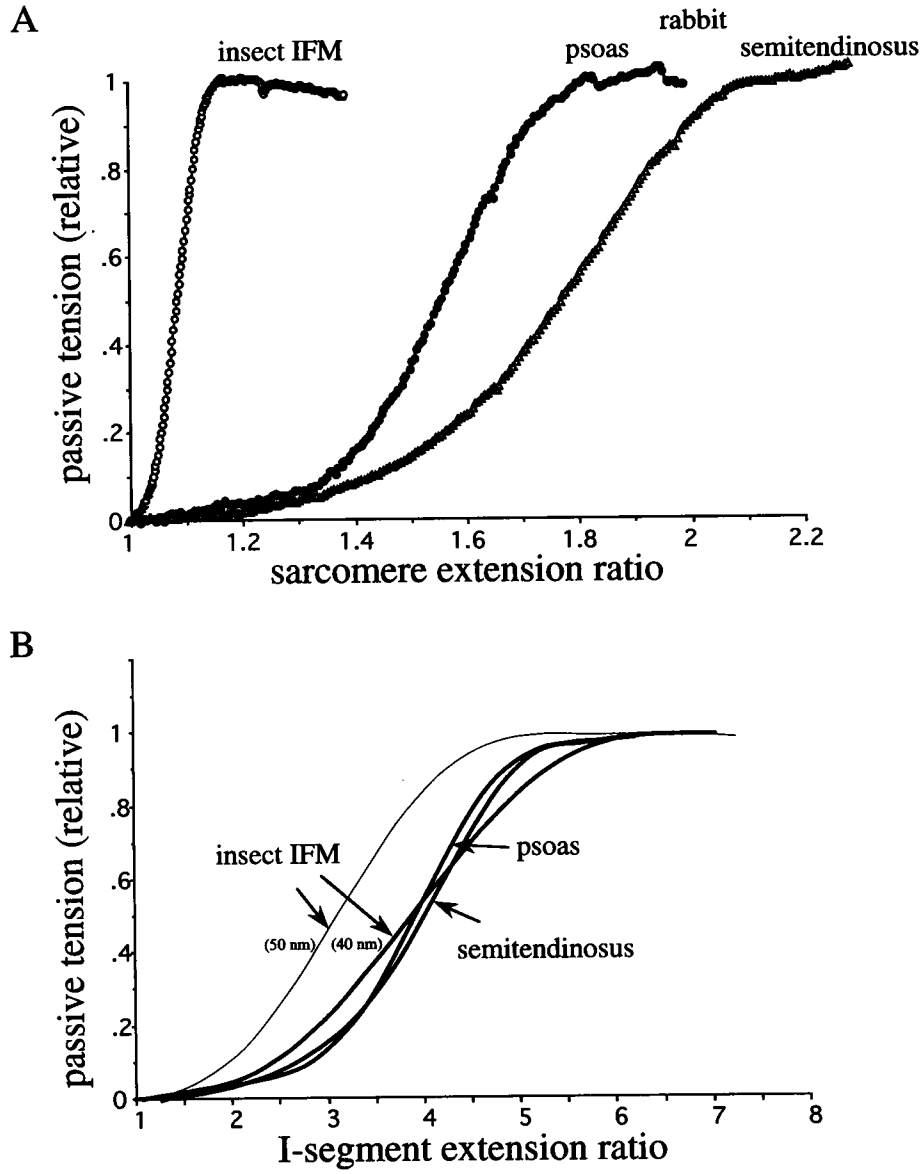

FIGURE 13 Tension-extension plots of IFM, psoas, and semitendinosus fibers. The first part of the second stretch cycle of Fig. 12 is shown for each fiber and tension is expressed relative to the plateau tension. (*A*) Tension versus sarcomere extension ratio (i.e., sarcomere length divided by slack sarcomere length). (*B*) Tension versus *I* segment extension ratio. The psoas and semitendinosus curves superimpose. Two curves are shown for IFM: one assumed a slack *I* segment length of 50 nm (*thin line*), the other assumed 40 nm (*thick line*).

(Kruger et al., 1991), possibly due to the calcium activation of endogenous calpains or contaminating proteases. These undesirable side effects occurred less frequently for insect IFM fibers (Granzier and Wang, 1993a). In our present study with an amino-terminal gelsolin fragment, FX-45 (45 kDa), actin filaments were removed without calcium (Yu et al., 1991) and without apparent undesirable side effects.

Gel analysis of fibers treated with FX-45 indicates that about 10–15% of total actin is resistant to extraction in both insect and psoas fibers (Figs. 1 and 2). F-actin labeling studies with rhodamine-phalloidin of both myofibrils and fibers revealed that Z-line actin is resistant to extraction. Actin outside the Z-line region is, however, completely removed in all sarcomeres (Figs. 3 and 4). The removal of thin-filament actin is also supported by the near complete abolishment of active and rigor tension after FX-45 treatment (Fig. 5).

The selectivity of FX-45 extraction is demonstrated by the observations that only actin and actin-associated proteins, such as troponin, tropomyosin, and arthrin were extracted (Figs. 1 and 2), while no other proteins were extracted or degraded. In particular, giant proteins such as titin, minititin, and nebulin remained essentially intact and unextracted.

In conclusion, Fx-45 is able to remove actin and its associated proteins from the thin-filament region of the sarcomere, without deleterious effects on the other proteins, including the megadalton proteins titin and nebulin that are notoriously sensitive to degradation (Wang, 1985). FX-45 is an ideal tool to specifically remove actin filaments from sarcomeres and evaluate the contribution of actin to tension and stiffness developed by muscle. Applications to other tissues can be anticipated.

Passive tension

In IFM fibers, passive tension was not affected by thin-filament removal (Fig. 6 and Table 2), confirming our earlier

conclusion that the thin filament and minititin are mechanically independent (Granzier and Wang, 1993a). In psoas fibers, however, passive tension was highly elevated after thin-filament removal (Fig. 7 and Table 2). A small increase in passive tension of psoas fibers has also been reported by Funatsu et al. (1990) after thin-filament removal with plasma gelsolin. The tension increase at 50% stretch amounted to about 10% in their study, much less than the 72% that we report here (Fig. 7 and Table 2). It is conceivable that the 2-h incubations with plasma gelsolin in the presence of 0.1 mM calcium (Funatsu et al., 1990) might have caused some degradation of titin thus lowering the level of tension enhancement below our values obtained with FX-45. Differences in mechanical protocols may also contribute to the discrepancy.

Despite that thin-filament removal from psoas fibers affects passive tension quantitatively, other basic features of the passive tension-sarcomere length relation remains unaffected by thin-filament removal, such as the initial exponentional tension rise (Fig. 7, *A* and *B*) and the sarcomere length at the yield point (Fig. 11 *A* and Table 2). Since the exponent, α, of exponential tension rise is not appreciably different in thin-filament free sarcomeres (Fig. 7 *B* and Table 2), it is likely that thin-filament removal may have caused a net reduction in the effective length of the extensible titin segment without any change in its intrinsic properties. It is relevant to note that thin-filament removal results in the formation of an electron-dense zone between the Z-line and the A band of rabbit psoas fibers (Funatsu et al., 1990; Granzier, Wright and Wang, unpublished observations). If such zone inhibits titin extensibility in its vicinity, then the remaining extensible segment would be effectively reduced in length. For a given sarcomere length the extensible segment would then be strained to a higher degree and thus develop a higher passive tension.

Theoretically, the increase in tension following thin-filament removal can be explained, if actin, or thin-filament proteins, interact with titin to depress passive tension. Alternatively, nebulin might interact with titin in thin filament-free sarcomeres, thus stiffening titin and enhancing tension at a given sarcomere length.

Passive stiffness and weak bridges

It is generally accepted that weak bridges exist in relaxed rabbit psoas fibers and can be detected mechanically as high frequency stiffness in the presence of MgATP (Brenner et al., 1982, 1991; Schoenberg, 1988). In relaxed psoas muscle these bridges are favored at low ionic strength, with approximately a 10-fold increase in the number when ionic strength decreases from 170 to 20 mM (Brenner et al., 1986). Weak bridges are thought to be obligatory precursors of force-generating bridges and are able to attach to actin in the absence of calcium but require calcium to enter a force generating cycle.

The existence of weak bridges in insect IFM fibers at physiological ionic strength (μ = 195 mM) and temperature (21–23°C) has been demonstrated with the thin-filament removal technique based on full length gelsolin (Granzier and Wang, 1993a). These conclusions are confirmed by FX-45-based extraction (Fig. 6), and are further extended by our experiments with caldesmon. The carboxyl-terminal (27 kDa) fragment of smooth muscle caldesmon, which inhibits weak cross-bridge interaction (Wang et al., 1991; Brenner et al., 1991), depresses stiffness of control fibers at 21–23°C and μ = 195 mM to a similar degree as that achieved by thin-filament removal (Fig. 6).

Similar experimental approaches were applied to search for evidence of weak bridges in rabbit psoas fibers at μ = 180 mM and 22°C. The gelsolin technique is less suitable for this purpose, since passive tension does not remain constant upon thin-filament removal (Fig. 7), making it difficult to attribute changes in passive stiffness following thin-filament removal entirely to actomyosin interaction. However, the caldesmon approach was successful in inhibiting a small but significant amount of weak bridge stiffness (5% of rigor stiffness) of control rabbit psoas fibers (Fig. 8). To our knowledge, this is the first report of weak bridges in rabbit psoas muscle under physiological conditions.

When ionic strength was lowered at low temperature, weak bridge stiffness increased significantly (Fig. 7), confirming previous reports by Brenner et al. (1982). To evaluate the dependence of weak bridge stiffness on the degree of overlap between thin and thick filaments, we adopted the assumption of Brenner et al. (1982), that the increase in stiffness that occurs at 5°C when the ionic strength is lowered from 170 to 20 mM is derived from weak bridges. We observed a nonlinear dependence of bridge stiffness on filament overlap: stiffness increased initially, reached a maximum at about 2.5 μm, then decreased modestly with sarcomere length to 3.2 μm and dropped rapidly to near zero at about 3.8 μm (Fig. 9 *C*). Additionally, the magnitude of weak bridge stiffness at a given sarcomere length is significantly higher after stretch than after release (Fig. 9 *C*). These data thus reveal some heretofore unappreciated complexities of weak bridge behavior.

It is conceivable that the fraction of bridges in the overlap zone that is in the weak bridge state is not constant over this range of filament overlap. Recently we proposed that the number of weak bridges (i.e., stiffness) in insect flight muscle is enhanced by passive tension (Granzier and Wang, 1993a). If a similar phenomenon occurs in rabbit psoas fibers, the weak bridge stiffness would be expected to be higher than that predicted from filament overlap between 2.4 and 3.1 μm, since passive tension increases exponentionally in this region. The rapid decline of stiffness between 3.1 and 3.6 μm might then result from the decrease in the rate of passive tension rise that occurs in this range and/or saturation of the fraction of bridges in the overlap zone that functions as weak bridge. The correlation between weak bridge stiffness and resting tension also holds for the release curve of Fig. 9 *C* (*dotted lines*): stiffness is much lower during release than during stretch and, similarly, passive tension during release is much lower due to hysteresis. It is interesting to

note that stiffness during the release curve of Fig. 9 *C* varies more closely with filament overlap than during stretch. This observation suggests that weak bridge stiffness may indeed decrease linearly with filament overlap when resting tension is below a low threshold value. This might explain the linear dependence between weak bridge stiffness and overlap in the study of Brenner et al. (1982). If passive tension serves to elevate the fraction of bridges in the weak bridge state then stiffness would indeed be higher than predicted from filament overlap, but still extrapolate to zero at nonoverlap (Fig. 9).

The relation between weak bridge stiffness and sarcomere length (Fig. 9 *C*) suggests that weak bridges should be explored at or above sarcomere lengths of 2.5 μm. These lengths, however, have been avoided in most studies reported earlier, presumably to minimize the contribution of titin filaments to passive stiffness (Brenner et al., 1982, 1986; Schoenberg, 1988; Bagni et al., 1992). We show that this issue can be dealt with satisfactorily by using stiffness-tension curves as a simple tool to dissect and evaluate the relative contribution of weak bridges and elastic filaments to stiffness (Figs. 6 *C* and 7 *D*).

The importance of passive tension in actomyosin interaction of insect indirect flight muscle has recently been reported and the finding was incorporated in a passive stress-activation model for insect muscle (Granzier and Wang, 1993a). Our current studies on rabbit psoas muscle point again to a mechanical coupling between passive tension and cross-bridge interaction. The extensible *I* segment of titin filaments may serve a dual role as generator of passive tension and as a stretch sensor for actomyosin interaction.

Segmental extension model of tension and stiffness of passive fibers

The segmental organization of titin formed the basis for a proposed segmental-extension model of passive tension development in vertebrate skeletal muscle (Wang et al., 1991, 1993). In this model, the titin segment in the *I* band is extensible and acts as an elastic connector that develops passive tension when the sarcomere is stretched. The remaining titin segment in the A band associates with the myosin filament and is normally prevented from extension. This segment can be recruited to contribute to passive tension when structural constraints are relieved, e.g., in sarcomeres that have been stretched beyond their elastic limit (Wang et al., 1991, 1993) or in sarcomeres from which myosin filaments have been selectively extracted (Higuchi et al., 1992). We have recently shown that the model is also applicable to insect indirect flight muscle, by assuming a short (~50 nm) extensible *I* segment of minititin as responsible for passive tension generation and an *A* segment (>200 nm) that can be recruited at high degrees of stretch (Granzier and Wang, 1993a).

In the present study, we extended the segmental extension concept by studying the passive tension as well as passive stiffness of insect IFM and two different rabbit muscles, psoas and semitendinosus, that express different size variants of titin and display different tension-length curves (Wang et al., 1991). We reinvestigated the tension-length behavior by stretching these fibers at the same *I* segment strain rate, and incorporated the simultaneous measurement of passive stiffness into the protocol.

Passive tension

Passive tension increases exponentially with sarcomere length and finally reaches a plateau that is maintained for some distance (Fig. 12). In the rabbit muscles, the plateau phase is followed by a second tension rise, which is likely to result from the intermediate filament system (Wang et al., 1991, 1993). In insect IFM, the plateau tension is maintained until the fiber breaks (5.3 μm). Absence of a second phase of tension rise, and the observation that KI extracted IFM fibers do not develop substantial tensions at long length (Fig. 12), suggest that intermediate filaments, if present at all, do not contribute to passive tension of IFM of *Lethocerus*.

The tension versus sarcomere extension plots of these three muscles differ substantially (Fig. 13 *A*). However, when tension is plotted versus *I* segment extension, curves of the two rabbit muscles superimpose. The IFM curve is brought close to those of rabbit muscles when a 50-nm *I* segment length is assumed, and all three curves nearly superimposes by assuming a 40-nm *I* segment length (Fig. 13 *B*). It is clear from these studies that *I* segment extension is a fundamental determinant of passive tension, as proposed by the segmental extension model.

The yield point in tension for each of the three muscles differs widely in sarcomere length (Fig. 13 *A*), but is found at a similar *I* segment extension ratio of about 5 (Fig. 13 *B*). This value is slightly higher that reported previously (Wang et al., 1991, 1993; Granzier and Wang, 1993a) which might result from the difference in strain rates and the use of the diffraction based slack length determination in the present study. It is striking that, despite major differences in sarcomere structure and molecular make-up of vertebrate skeletal and insect flight muscles, the yield-points are found at a similar *I* segment strain.

Passive stiffness

The passive stiffness-sarcomere length curves share many of the features of the passive tension curves, such as the initial exponential rise, a maximum at the yield point, and hysteresis upon release (Fig. 12). Closer comparison, however, revealed subtle but prevailing differences. For example, the stiffness yield point occurs at a sarcomere length that is shorter than the tension yield point, and post-yield point stiffness drops significantly, whereas tension remains relatively constant (Figs. 12, *A* and *B*).

Plots of passive tension versus passive stiffness are multiphasic and consist of several linear segments that are strikingly similar for the three muscle types (Fig. 12 *C*). A transition point around 40–50 kN m^{-2} corresponds to the

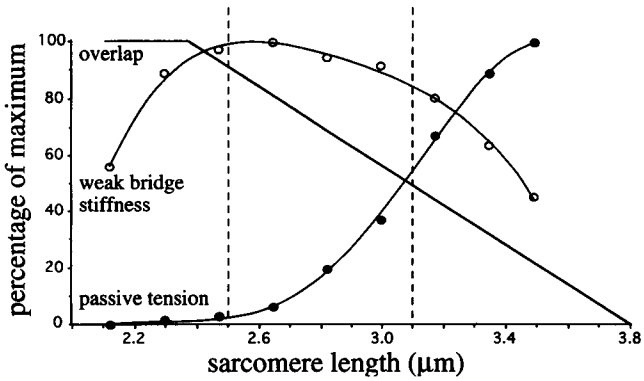

FIGURE 14 Sarcomere length dependence of weak bridge stiffness and passive tension. Weak bridge stiffness (*open circles* ΔE at the end of each stretch in Fig. 9) and passive tension (*closed circles*, from experiments in Fig. 9) of the same rabbit psoas fiber were plotted together with the degree of thin-thick filament overlap (*solid lines*), as a function of sarcomere length. Three phases can be recognized in both stiffness and tension curves. The similarity in the sarcomere lengths at which transitions occur suggests a mechanical coupling between weak bridge and passive tension.

sarcomere length at which tension starts to deviate from exponential rise, a second transition point that signals a precipitous drop near 100–130 kN m^{-2}, corresponds to the yield point of stiffness. The curve below 40–50 kN m^{-2} can also be resolved into two linear segments with a transition near 10–20 kN m^{-2}. The structural basis for these transitions remains to be elucidated, although it is clear that similar transitions occur in the absence of the thin filament (Fig. 11 *C*) and do no require nebulin since they are found in IFM fibers (Fig. 12 *C*). It is tempting to speculate that both minititin and titin consist of similar types of mechanical units. The common dual-sequence motif structure of minititin (Ayme-Southgate, 1991) and titin (Labeit et al., 1992) may underlay this mechanical similarity. It is worth noting that dynamic stiffness is a more sensitive indicator than tension to detect the onset of structural changes that occur near the yield point (Fig. 12). The simultaneous measurement of both passive tension and stiffness allows stiffness-tension plots to be used as a highly discriminating tool to reveal various structural transitions and mechanical events within the pre-yield region, near the yield point and during post-yield stretch of the stress-strain curves of passive muscles.

The possible mechanical coupling between weak bridge stiffness and passive tension is illustrated in Fig. 14 in which their sarcomere length dependence was compared. Three phases can be recognized in both curves: 1) between 2.2 and 2.5 μm, weak bridge stiffness increase linearly, while passive tension rises gradually; 2) between 2.5 and 3.1 μm, weak bridge stiffness declines moderately, while tension rise exponentially; 3) between 3.1 and 3.6 μm, stiffness decreases rapidly, while tension begins to deviate from exponential and reaches a maximum at the yield point. The similarity in the sarcomere lengths at which these transitions occur suggests a coupling of these two mechanical parameters.

We express our gratitiude to Dr. H. Yin for her generous gift of the FX-45 clone and helpful advice of its purification, and to Dr. Albert Wang for his generous gift of smooth muscle caldesmon fragment. We thank Dr. K. Diller for the use of the Zeiss confocal microscope.

This work is supported by grants from National Institutes of Health (DK 20270 to K. Wang), Foundation for Research (to K. Wang), and a Neuromuscular Disease Research Fellowship from the Muscular Dystrophy Association of America (to H. Granzier).

REFERENCES

Ayme-Southgate, A., J. Vigoreaux, G. Benian, and M. L. Pardue. 1991. Drosophila has a twitchin/titin-related gene that appears to encode projectin. *Proc. Natl. Acad. Sci. USA.* 88:7973–7977.

Bagni, M. A., G. Cecchi, F. Colomo, P. Garzella. 1992. Are weakly binding bridges present in resting intact muscle fibers? *Biophys. J.* 63:1412–1415.

Benian, G. M., J. E. Kiff, N. Neckelman, D. G. Moerman, and B. Waterston. 1989. Sequence of a large protein implicated in regulation of myosin activity in C. elegans. *Nature (Lond.).* 342:45–50.

Brenner, B., J. M. Chalovich, L. E. Greene, E. Eisenberg, and M. Schoenberg 1986. Stiffness of skinned rabbit psoas fibers in MgATP and MgPP solution. *Biophys. J.* 50:685–691.

Brenner, B., L. C. Yu, and J. M. Chalovich. 1991. Parallel inhibition of active force and relaxed fiber stiffness in skeletal muscle by caldesmon: implications for the pathway to force generation. *Proc. Natl. Acad. Sci. USA.* 88:5739–5743.

Brenner, B., M. Schoenberg, J. Chalovich, L. Greene, and E. Eisenberg. 1982. Evidence for cross-bridge attachment in relaxed muscle at low ionic strength. *Proc. Natl. Acad. Sci. USA.* 79:7288–7291.

Fabiato, A. 1988. Computer programs for calculating total from specified free or free from specified total ionic concentrations in aqueous solutions containing multiple metals and ligands. *Methods Enzymol.* 157:378–417.

Fairbanks, G., T. L. Steck, and D. F. H. Wallach. 1971. Electrophoretic analysis of the major polypeptides of the human erythrocyte membrane. *Biochemistry.* 10:2606–2617.

Funatsu, T., T. H. Higuchi, and S. Ishiwata. 1990. Elastic filaments in skeletal muscle revealed by selective removal of thin filaments with plasma gelsolin. *J. Cell Biol.* 110:53–62.

Granzier, H., and K. Wang. 1993a. Interplay between passive tension and strong and weak binding cross-bridges in insect indirect flight muscle. *J. Gen. Physiol.* 101:235–270.

Granzier, H., and K. Wang. 1993b. Gel electrophoresis of giant proteins: solubilization and silver-staining of titin and nebulin from single muscle fiber segments. *Electrophoresis.* 14:56–64.

Granzier, H., J. Myers, and G. Pollack. 1987. Stepwise shortening of muscle fiber segments. *J. Muscle Res. Cell Motil.* 8:242–251.

Greaser, M. L., and B. E. Schnasse. 1990. Non-uniform binding of phalloidin to myofibrils thin filaments. *J. Cell. Biochem. Suppl.* 14A:13. (Abstr.)

Higuchi, H., T. Suzuli, S. Kimura, S. Yoshioka, K. Maruyama, and Y. Umazuma. 1992. Localization and elasticity of connectin (titin) filaments in skinned frog muscle fibers subjected to partial depolymerization of thick filaments. *J. Muscle Res. Cell Motil.* 13:285–294.

Hu, D. H., A. Mutsuno, K. Terakado, T. Matsuura, S. Kimura, and K. Maruyama 1990. Projectin is an invertebrate connectin (titin): isolation from crayfish claw muscle and localization in crayfish claw muscle and insect flight muscle. *J. Muscle Res. Cell Motil.* 11:497–511.

Jin, J. P., and K. Wang. 1991. Nebulin as a giant actin-binding template protein in skeletal muscle sarcomere. Interaction of actin and cloned human nebulin fragments. *FEBS Lett.* 281:93–96

Kruger, M., J. Wright, and K. Wang. 1991. Nebulin as a length regulator of thin filaments of vertebrate skeletal muscle: correlation of thin filament length, nebulin size, and epitope profile. *J. Cell Biol.* 115:97–107.

Labeit, S., M. Gautel, A. Lackey, and J. Trinick. 1992. Towards a molecular understanding of titin. *EMBO J.* 11:1711–1716.

Laemmli, U. K. 1970. Cleavage of structural proteins during the assembly of the head of bacteriophage T4. *Nature (Lond.).* 227:680–685.

Lakey, A., C. Ferguson, S. Labeit, M. Reedy, A. Larkins, G. Butcher, K. Leonard, and B. Bullard. 1990. Identification and localization of high molecular weight proteins in insect flight and leg muscle. European Molecular Biology Journal. 9:3459–3467.

Maruyama, K. 1986. Connectin, an elastic protein of striated muscle. *Int. Rev. Cytol.* 104:81–114.

Nave, R., and K. Weber. 1990. A myofibrillar protein of insect muscle related to vertebrate titin connects Z band and A band: purification and molecular characterization of invertebrate minititin. *J. Cell Sci.* 95:535–544.

Nave, R., D. Furst, U. Vinkemeier, and K. Weber. 1991. Purification and physical properties of nematode minititins and their relation to twitchin. *J. Cell Sci.* 98:491–496.

Reedy, M. K. 1971. Electron microscope observations concerning the behavior of the cross-bridge in restricted muscle. *In* Symposium on Contractility. R. J. Podolsky, editor. Prentice Hall, Englewood Cliffs, New Jersey. 229–246.

Schoenberg, M. 1988. Characterization of the myosin adenosine triphosphate (M. ATP) crossbridge in rabbit and frog skeletal muscle fibers. *Biophys. J.* 54:135–148.

Trinick, J. 1991. Elastic filaments and giant proteins in muscle. *Curr. Opin. Cell Biol.* 3:112–118.

Trombitas, K., and Tigyi-sebes 1979. The continuity of thick filaments between sarcomeres in honey-bee flight muscle. *Nature (Lond.).* 281: 319–320.

Wang, C.-L. A., L.-W. C. Wang, S. Xu, R. C. Lu, V. Saavedra-Alanis, and J. Bryan. 1991. Localization of the calmodulin- and the actin-binding sites of caldesmon. *J. Biol. Chem.* 266(14):9166–9172.

Wang K. 1985. Sarcomere-associated cytoskeletal lattices in striated muscle. *Cell Muscle Motil.* 6:315–369.

Wang, K., and R. Ramirez-Mitchell. 1983. A network of transverse and longitudinal intermediate filaments is associated with sarcomeres of adult vertebrate skeletal muscle. *J. Cell Biol.* 96:562–570.

Wang, K., and C. Williamson. 1980. Identification of an N2 line protein of striated muscle. *Proc. Natl. Acad. Sci. USA.* 77:3254–3258.

Wang, K., and J. Wright. 1988. Architecture of the sarcomere matrix of skeletal muscle: immunoelectron microscopic evidence that suggests a set of parallel inextensible nebulin filaments anchored at the Z-line. *J. Cell Biol.* 107:2199–2212

Wang, K., R. McCarter, J. Wright, B. Jennate, R. Ramirez-Mitchell. 1991. Regulation of skeletal muscle stiffness and elasticity by titin isoforms. *Proc. Natl. Acad. Sci. USA.* 88:7101–7109.

Wang, K., R. McCarter, Wright, J., B. Jennate, and R. Ramirez-Mitchell. 1993. Viscoelasticity of the sarcomere matrix of skeletal muscles: the titin-myosin composite filament is a dual-range molecular spring. *Biophys. J.* 84:1161–1177.

White, D. C. S., and J. Thorson. 1973. The kinetics of muscle contraction. *Prog. Biophys. Mol. Biol.* 27:175–255.

White, D. C. S., 1983. The elasticity of relaxed insect fibrillar flight muscle. *J. Physiol. (Lond.)* 343:31–57.

Wilson, P., E. Fuller, and A. Forer. 1987. Irradiations of rabbit myofibrils with an ultraviolet microbeam. II. Phalloidin protects actin in solution but not in myofibrils from depolymerization by ultraviolet light. *Biochem. Cell Biol.* 65:376–385.

Wright, J., Q. Q. Huang, K. Wang. 1993. Nebulin is a full-length template of actin filaments in skeletal muscle sarcomeres: an immuno-electron microscopic study of its orientation and span with site-specific monoclonal antibodies. *J. Muscle Res. Cell Motil.* In press.

Yu, F. X., D. Zhou, and H. L. Yin. 1991. Chimeric and truncated gCap39 elucidate the requirements for actin filament severing and end capping by the gelsolin family of proteins. *J. Biol. Chem.* 266:19269–19275.